Mathematics

https://www.aimspress.com/journal/Math

AIMS Mathematics, 11(9): 28348–28382.
DOI: 10.3934/math.20261129
Received: 02 June 2026
Revised: 18 August 2026
Accepted: 24 August 2026
Published: 04 September 2026

Research article

An exact gamma–beta scale-mixture law for the squared norm of a complex-Gaussian-scaled sum of hyperspherical random vectors

Ki-Hun Lee[1] **and Nam-Jin Park**[2,*]

[1] Department of Electronics and Information Engineering, Korea University, Sejong, 30019, South Korea

[2] Department of Control and Instrumentation Engineering, Pukyong National University, Busan, 48513, South Korea

* **Correspondence:** Email: pnj@pknu.ac.kr.

Abstract: We derive the exact probability distribution of the squared norm of a sum of complex-Gaussian-scaled hyperspherical random vectors. The derived law reveals a new gamma–beta scale-mixture representation for this random norm, expressing it as the product of a gamma-distributed squared norm of an isotropic complex Gaussian vector and a compactly supported weighted sum of independent beta random variables. As a concrete engineering application, this distribution arises as the effective channel gain of fully distributed space–time block coding (FD-STBC) systems with independent complex unit-hyperspherical signatures for arbitrary numbers of transmitters K and underlying orthogonal space–time block coding (STBC) dimensions L. On the basis of the representation, we obtain a fully expanded density for the mixing variable, finite-sum closed-form expressions for the probability density function (PDF) and cumulative distribution function (CDF) of the effective channel gain, an exact Laplace transform, and closed-form moments. Furthermore, we apply the derived distribution to the FD-STBC system and obtain analytical expressions for outage probability and bit error rate (BER), together with a high signal-to-noise ratio (SNR) asymptotic expansion that yields the diversity order $\min(K, L)$. Numerical experiments show close agreement between the analytical results and Monte Carlo simulations for both the derived distribution and the associated performance metrics.

Keywords: exact probability distribution; scale-mixture distribution; gamma–beta scale-mixture law; weighted beta sum; hyperspherical random vectors; fully distributed space–time block coding
Mathematics Subject Classification: 60E05, 60E10, 62E15, 94A05

1. Introduction

Mathematical modeling of real-world engineering systems often involves random internal mechanisms. Although these mechanisms can be straightforward to implement in a simulator, analytically characterizing the probability law induced by the overall system model can be difficult, even when the distributions of the constituent random variables are known. Monte Carlo simulation is therefore widely used to evaluate system performance. Nevertheless, analytical characterization remains important because it complements simulation results and supports systematic parameter studies and model-based design. A related example in wireless communications is the derivation of largest-eigenvalue distributions for complex Wishart matrices to analyze the outage probability of multiple-input multiple-output (MIMO) channels [1]. Motivated by this line of distributional analysis, we consider the following problem: The squared norm of a random vector obtained by summing complex-Gaussian-scaled hyperspherical random vectors. Although classical beta, gamma, and Dirichlet laws provide the elementary components of this construction [2,3], their coupling through random vector summation and the squared-norm operation leads to a nonstandard distribution outside the usual families of tractable probability laws.

Space–time block coding (STBC) is a classical spatial-diversity technique for MIMO wireless communication systems, providing full diversity with low-complexity linear decoding [4, 5]. Distributed STBC (D-STBC) extends this principle to geographically separated cooperating transmitters, but such schemes generally require node-specific code-column or signature-vector assignments [6–8]. Such assignments entail network-wide coordination and signaling overhead. Randomized space–time coding (R-STC) avoids this requirement by allowing each transmitter to independently generate a random signature vector and transmit a linear combination of the columns of a common STBC codeword [9]. We refer to this coordination-free realization as fully distributed STBC (FD-STBC) throughout the paper [10].

Among several randomization methods for FD-STBC, selecting signature vectors uniformly on the complex unit hypersphere is particularly attractive. The resulting unit-norm signatures provide a practical form of inherent per-node transmit power normalization. Hyperspherical randomization has also been reported to yield favorable error rate performance [9]. However, this unit-norm constraint induces a nonstandard product-and-sum structure in the post-combining effective channel gain, making its exact distribution difficult to characterize. Therefore, an exact characterization of the effective channel gain distribution is needed to evaluate communication performance metrics without relying on repeated Monte Carlo simulations over the underlying random signatures and wireless channel coefficients.

1.1. Related work

1.1.1. Distribution theoretic perspective

From a distribution theoretic perspective, the analysis of the effective channel gain in the considered FD-STBC model draws on classical beta, gamma, and Dirichlet laws and is also related to product distributions and sums of beta-type random variables. For a random vector uniformly distributed on the complex unit hypersphere, the squared magnitude of its projection onto any fixed unit direction follows a beta distribution, and the squared magnitudes of its normalized coordinates are governed by a Dirichlet law. This hyperspherical and directional–statistical background is closely related to the general theory of distributions on spheres [11]. In addition, the squared norm of a complex Gaussian vector has a gamma distribution [2, 3]. Products of independent beta, gamma, and Gaussian random variables have also been studied through Meijer G-function representations [12, 13], and tail asymptotics for the products of independent beta and generalized gamma random variables have been characterized [14]. These results provide useful elementary components but they primarily concern scalar products or the asymptotic tail behavior and do not directly yield the exact unconditional distribution of the random vector norm arising in FD-STBC.

The present problem is also connected to the distribution of sums and linear combinations of independent beta random variables. In a broader multivariate setting, linear combinations of Dirichlet components have been represented through integral formulas [15], suggesting that exact finite-dimensional distributional reductions often require carefully exploited structural constraints. However, the relevant linear combination is formed from the dependent components of a single Dirichlet random vector, whereas the present construction involves independent projection variables generated by different hyperspherical signatures. Closed-form expressions are available in special low-dimensional cases, such as the linear combination of two independent general beta variables [16], whereas the sums of more than two independent beta variables have been treated using approximation methods, including saddlepoint approximations [17]. Related mixed-sum models involving gamma and beta random variables have been studied in an availability-motivated setting [18], including gamma–beta product structures under particular parameter relationships. The gamma–beta construction in that work starts from a sum of products involving beta and gamma variables, rather than from a deterministically weighted sum of independent beta projection variables multiplied by a common independent gamma radial factor.

These neighboring results do not directly yield the scale-mixture distribution considered in this paper. Specifically, the effective channel gain of FD-STBC is not merely a weighted beta sum. As shown later, it admits the coupled scale-mixture representation $Z \overset{d}{=} G_L \sum_{k=1}^{K} \sigma_k U_k$, where G_L is gamma-distributed, $\sigma_k > 0$, and the variables U_k are independent Beta$(1, L-1)$ random variables. The present model differs in that the random scale is the weighted sum $A = \sum_{k=1}^{K} \sigma_k U_k$ of independent Beta$(1, L-1)$ variables with deterministic channel-power weights. This weighted beta sum is induced by the isotropic vector summation of independent hyperspherical signatures. For $K \geq 2$, A does not, in general, reduce to a single scaled beta random variable and cannot be gamma-distributed because its support is compact. For integer $L \geq 2$, its density is piecewise polynomial, with possible breakpoints at subset sums of the weights $\{\sigma_k\}$. Consequently, deriving the distribution of Z requires two steps: An explicit characterization of the compactly supported weighted beta sum and a subsequent gamma-mixture integration. Thus, except for special reductions such as $K = 1$, the resulting law is not a reparameterization of a classical scalar gamma–beta product. To the best of our knowledge, finite-sum closed-form expressions for the exact unconditional probability density function (PDF) and cumulative distribution function (CDF) of Z have not been reported.

1.1.2. Communication engineering perspective

Table 1 summarizes the studies most directly related to the present work and classifies them by system model, channel model, signature vector distribution, and type of analytical result. Here, SEP, BER, and APEP denote symbol error probability, bit error rate, and average pairwise error probability, respectively. The abbreviations DF, AF, and BRN denote decode-and-forward, amplify-and-forward, and barrage relay network, respectively. The reviewed studies fall broadly into three groups. The first uses complex Gaussian signatures, whereas the second compares multiple randomization strategies but provides only diversity-order or bound-based results. The third focuses on hyperspherical signatures or isometrically randomized coding matrices.

Much of the existing FD-STBC-related literature has adopted complex Gaussian signatures because this assumption leads to a relatively tractable performance characterization. Verde et al. [19] developed a cooperative randomized multicell multiple-input multiple-output orthogonal frequency-division multiplexing (MIMO-OFDM) downlink framework and derived analytical upper bounds on the SEP under linear receivers. For FD-STBC over relay channels, Duong et al. [20] obtained exact closed-form SEP and outage probability expressions under Rayleigh fading, while Soffritti et al. [21] extended exact SEP and outage analysis to Nakagami-m fading. This line of work was later extended to composite gamma/lognormal fading in [22]. That study derived tight analytical approximations for SEP and outage probability, together with a high signal-to-noise ratio (SNR) SEP expression, for FD-STBC with complex Gaussian signatures. Alay et al. [23] incorporated FD-STBC into cooperative layered video multicast and evaluated cross-layer reliability using BER-based packet delivery and video rate metrics. These studies provide valuable Gaussian randomization performance results, but they do not address unit-norm hyperspherical signatures, which are attractive in terms of inherent per-node transmit power normalization and favorable error rate performance.

Table 1. Summary of studies most directly related to the present work.

Reference	System model	Channel model	Signature vector distribution	Analysis results
[9]	Direct cooperative transmission	Rayleigh fading	Gaussian, uniform phase, unit hypersphere	Diversity order; numerical for the hypersphere case
[20]	DF relay	Rayleigh fading	Complex Gaussian	Exact SEP and outage
[24]	AF relay	Rayleigh fading	Gaussian, uniform phase, hypersphere	APEP upper bounds, diversity order
[25]	DF relay	Rayleigh fading	Haar/isometric coding matrices	Spectral efficiency; large-matrix analysis
[10]	BRN with two relays and Alamouti code	Rayleigh fading	Complex unit hypersphere	Outage upper bound (approximation)
Proposed	Direct cooperative transmission	Rayleigh fading	Complex unit hypersphere	Exact closed-form PDF, CDF, BER, outage

A second line of work has compared different signature vector randomization rules in FD-STBC. A pioneering work in this direction is that of Sirkeci-Mergen and Scaglione [9], who introduced R-STC and compared complex Gaussian, real Gaussian, uniform phase, and hyperspherical randomization rules. They characterized the achievable diversity order and showed numerically that complex unit-hyperspherical randomization can provide particularly favorable error rate performance, but the exact unconditional distribution of the effective channel gain under hyperspherical randomization was not derived. Verde [24] analyzed AF distributed STBC with Gaussian, uniform phase, and hyperspherical randomization and derived APEP upper bounds and diversity order results. These works provide diversity characterizations and performance bounds for several randomization rules, but they do not provide the exact unconditional PDF and CDF of the effective channel gain induced by independent complex unit-hyperspherical signatures.

A few works are more directly related to hyperspherical signatures or isometrically randomized coding matrices. Lee et al. [10] considered complex unit-hyperspherical signatures in an FD-STBC scheme for BRNs and demonstrated significant gains over conventional phase rotation-based cooperation. Their analysis, however, was restricted to two transmitters and the Alamouti code, the simplest two-antenna orthogonal STBC [5]. The resulting outage characterization was an approximate upper bound rather than an exact distributional formula. Gregoratti et al. [25] proposed a randomized isometric linear dispersion STBC for a DF relay channel, where the coding matrices are Haar/isometrically distributed. The columns of such matrices are marginally uniform on the complex unit hypersphere, but they are coupled through orthogonality and therefore differ from the independent hyperspherical signatures considered here. Moreover, their results concern spectral efficiency and large-matrix asymptotics rather than the exact unconditional distribution of the effective channel gain. To the best of our knowledge, the exact unconditional distribution of the effective channel gain under independent complex unit-hyperspherical signatures remains unavailable for arbitrary numbers of transmitters and orthogonal STBC dimensions.

1.2. Contributions

To bridge the aforementioned theoretical and computational gap, we derive the exact unconditional distribution of the effective channel gain for FD-STBC with an arbitrary number of active transmitters and arbitrary underlying orthogonal STBC (O-STBC) dimensions. Instead of relying on the eigenvalue distribution of the random Gram matrix induced by hyperspherical signatures, the proposed analysis directly characterizes the effective channel vector and reveals a gamma–beta scale-mixture representation. This representation yields finite-sum closed-form expressions for the PDF, CDF, outage probability, and BER. These expressions provide a deterministic alternative to repeated Monte Carlo averaging for the considered metrics and an analytical basis for parameter studies of FD-STBC systems with hyperspherical signatures. The contributions of this paper are summarized as follows.

- We formulate the effective channel gain of FD-STBC with independent complex unit-hyperspherical signatures as an exact distributional problem induced by the squared norm of a sum of complex-Gaussian-scaled hyperspherical random vectors.
- Denoting this effective channel gain by Z, we prove the exact gamma–beta scale-mixture law $Z \overset{d}{=} AG_L$, where A is a weighted sum of independent $\mathrm{Beta}(1, L-1)$ random variables and $G_L \sim \mathrm{Gamma}(L, 1)$. On the basis of this representation, we derive a fully expanded expression for the density of A and finite-sum closed-form expressions for the PDF and CDF of Z. We also derive its exact Laplace transform and closed-form moments.
- We use the derived distribution to analyze communication performance by obtaining deterministic analytical expressions for the outage probability and BER. We further derive the high-SNR outage expansion and show that the diversity order of FD-STBC is $\min(K, L)$, where K is the number of transmitters and L is the number of underlying O-STBC dimensions.

- We compare the derived distribution and performance expressions with Monte Carlo experiments for the PDF of effective channel gain, outage probability, high-SNR diversity behavior, and BER. The results demonstrate that the analytical formulas provide deterministic evaluations that agree with repeated averaging over random signatures and fading realizations.

1.3. Notation

Throughout this paper, $|\cdot|$ and $\|\cdot\|$ denote the absolute value and Euclidean norm, respectively. The transpose and Hermitian transpose are denoted by $(\cdot)^{\mathrm{T}}$ and $(\cdot)^{\mathrm{H}}$, respectively. The all-zero vector is denoted by $\mathbf{0}$, the $n \times n$ identity matrix by $\mathbf{I}_n$, the complex field by $\mathbb{C}$, the non-negative real line by $\mathbb{R}_+$, and the set of non-negative integers by $\mathbb{Z}_+$. The imaginary unit is denoted by $j = \sqrt{-1}$, and the real part of a complex number is denoted by $\mathrm{Re}\{\cdot\}$. For the matrices, $\det(\cdot)$ and $\mathrm{diag}(\cdot)$ denote determinant and diagonal matrix construction, respectively. For a finite set $\mathcal{T}$, $|\mathcal{T}|$ denotes its cardinality and $\varnothing$ denotes the empty set. For a finite-dimensional multi-index $\mathbf{v} = (v_1, \ldots, v_d)$, $|\mathbf{v}| = \sum_{\ell=1}^{d} v_\ell$. We use $\triangleq$ for definitions, $\overset{d}{=}$ for equality in distribution, and $X \sim \mathcal{D}$ to indicate that X follows distribution $\mathcal{D}$. In asymptotic statements, $g(x) \sim h(x)$ means $g(x)/h(x) \to 1$, and $O(\cdot)$ has its standard Landau meaning. We write $\overset{d}{\to}$ and $\xrightarrow{\text{a.s.}}$ for convergence in distribution and almost sure convergence, respectively.

The operators $\Pr(\cdot)$ and $\mathbb{E}[\cdot]$ denote probability and expectation, respectively. For a random variable X, $f_X(\cdot)$, $F_X(\cdot)$, and $\mathcal{L}_X(\cdot)$ denote its PDF, CDF, and Laplace transform, respectively. The distributions $\mathcal{CN}(\boldsymbol{\mu}, \Sigma)$, $\mathrm{Gamma}(\cdot,\cdot)$, $\mathrm{Beta}(\cdot,\cdot)$, $\mathrm{Exp}(\cdot)$, and $\mathrm{Dirichlet}(\cdot)$ denote the circularly symmetric complex Gaussian law, gamma law, beta law, exponential law, and Dirichlet law, respectively. In particular, $\mathcal{CN}(\boldsymbol{\mu}, \Sigma)$ has mean $\boldsymbol{\mu}$ and covariance Σ. The gamma distribution is parameterized by shape α and rate β; that is, if $X \sim \mathrm{Gamma}(\alpha,\beta)$, then $f_X(x) = \beta^\alpha x^{\alpha-1} e^{-\beta x}/\Gamma(\alpha)$, $x \geq 0$. The functions $\mathrm{erfc}(\cdot)$, $\Gamma(\cdot)$, $\Gamma(\cdot,\cdot)$, ${}_2F_1(\cdot)$, and $F_A^{(K)}(\cdot)$ denote the complementary error function, gamma function, upper incomplete gamma function, Gauss hypergeometric function, and Lauricella hypergeometric function of Type A, respectively. Note that the notation $F_A^{(K)}$ is Lauricella's function, not the CDF of a random variable A. Finally, $\binom{\cdot}{\cdot}$, $\lfloor\cdot\rfloor$, $(x)_n = \Gamma(x+n)/\Gamma(x)$, and $(x)_+ = \max(x, 0)$ denote the binomial coefficient, floor function, Pochhammer symbol, and positive part operator, respectively.

2. System model and problem statement

2.1. FD-STBC signal model

We consider a distributed cooperative transmission from K single-antenna transmitters to one receiver. In relay system interpretations, the present model corresponds to the cooperative transmission phase after the forwarding nodes have been determined [9]. DF protocols can then be incorporated by conditioning on the decoding success relay set and averaging over first-hop success events, whereas AF protocols require combining the derived second-hop distribution with the corresponding first-hop SNR and amplification rule. The transmitter set is $\mathcal{K} = \{1, 2, \ldots, K\}$. All transmitters send the same information-bearing vector $\mathbf{x} = [x_1, \ldots, x_N]^{\mathrm{T}}$, where the entries are normalized M-ary quadrature amplitude modulation (M-QAM) symbols satisfying $\mathbb{E}[|x_n|^2] = 1$. The integer $N \geq 2$ denotes the number of information symbols carried by one space–time block codeword.

Let $\mathcal{B}_{N/T}^{L}(\mathbf{x}) \in \mathbb{C}^{T \times L}$ denote a rate-N/T orthogonal STBC (O-STBC) codeword generated from $\mathbf{x}$, and write $\mathcal{B}(\mathbf{x}) = \mathcal{B}_{N/T}^{L}(\mathbf{x})$ for notational brevity. The $T \geq 2$ rows correspond to symbol intervals or channel uses within one codeword, and the $L \geq 2$ columns correspond to the virtual transmit dimensions of the underlying O-STBC. We use a generalized complex O-STBC [4,26] satisfying

$$\mathcal{B}(\mathbf{x})^{\mathrm{H}}\mathcal{B}(\mathbf{x}) = \|\mathbf{x}\|^2\mathbf{I}_L. \tag{2.1}$$

In the considered FD-STBC system, node k maps the common symbols $\mathbf{x}$ onto the same predefined O-STBC codeword $\mathcal{B}(\mathbf{x})$ and transmits the length-T block vector $\mathcal{B}(\mathbf{x})\mathbf{r}_k$, where $\mathbf{r}_k = [r_{k,1}, \ldots, r_{k,L}]^{\mathrm{T}} \in \mathbb{C}^L$ is its randomization or signature vector. This block vector is a random linear combination of the L codeword columns; equivalently, at each symbol interval, the transmitted scalar is the inner product between the corresponding row of $\mathcal{B}(\mathbf{x})$ and $\mathbf{r}_k$. The received signal vector $\mathbf{y} = [y_1, \ldots, y_T]^{\mathrm{T}}$ is

$$\mathbf{y} = \sum_{k=1}^{K} \sqrt{P_k}\sqrt{\delta_k^{-\alpha}}\tilde{h}_k\mathcal{B}(\mathbf{x})\mathbf{r}_k + \mathbf{w}, \tag{2.2}$$

where δ_k is the distance from node k to the receiver, α is the path-loss exponent, and $\delta_k^{-\alpha}$ represents the large-scale fading component. The normalized small-scale fading coefficients $\tilde{h}_k$, $k \in \mathcal{K}$, are modeled as independent and identically distributed (i.i.d.) circularly symmetric complex Gaussian random variables, $\tilde{h}_k \sim \mathcal{CN}(0,1)$, so that the corresponding envelopes follow Rayleigh fading. We define $h_k = \sqrt{\delta_k^{-\alpha}}\tilde{h}_k$, so that $h_k \sim \mathcal{CN}(0,\sigma_k)$ with $\sigma_k = \delta_k^{-\alpha}$. Thus, $|h_k|^2$ is exponentially distributed with mean σ_k. More generally, all subsequent distributional results hold for arbitrary positive average channel powers $\sigma_k > 0$. The additive white Gaussian noise (AWGN) vector is $\mathbf{w} \sim \mathcal{CN}(\mathbf{0}, N_0\mathbf{I}_T)$.

Each signature vector $\mathbf{r}_k$ is uniformly distributed on the complex unit hypersphere in $\mathbb{C}^L$. Equivalently, one may generate $\mathbf{r}_k = \tilde{\mathbf{r}}_k/\|\tilde{\mathbf{r}}_k\|$, where $\tilde{\mathbf{r}}_k \sim \mathcal{CN}(\mathbf{0}, \mathbf{I}_L)$. Hence $\|\mathbf{r}_k\|^2 = 1$ almost surely. The signature vectors $\mathbf{r}_1, \ldots, \mathbf{r}_K$ are mutually independent and are also independent of $h_1, \ldots, h_K$. The mutual independence of the signature vectors does not imply mutual orthogonality; the realized signatures are generally nonorthogonal, with their geometric overlap quantified later in Corollary 3.8 by $\mathbb{E}[|\mathbf{r}_i^{\mathrm{H}}\mathbf{r}_j|^2] = 1/L$ for $i \neq j$. The coefficient P_k denotes a codeword-level power-scaling coefficient applied before the O-STBC codeword. For a rate-N/T O-STBC, the unscaled block $\mathcal{B}(\mathbf{x})\mathbf{r}_k$ has normalized time-averaged power N/T. Hence, to achieve a prescribed actual time-averaged transmit power, the codeword-level scaling coefficient must compensate for this factor by T/N. Specifically, using (2.1) and $\|\mathbf{r}_k\|^2 = 1$, we obtain

$$\mathbb{E}_{\mathbf{x}}\left[\frac{1}{T}\left\|\mathcal{B}_{N/T}^{L}(\mathbf{x})\mathbf{r}_k\right\|^2\right] = \frac{N}{T}. \tag{2.3}$$

Furthermore, to focus on the distributional effect of hyperspherical signatures, we use a common power-scaling coefficient for all transmit nodes. Specifically, the total time-averaged transmit power of the network is fixed as P_{tot}, and each node has an average transmit power P_{tot}/K. Therefore, to make the actual time-averaged power of node k equal to P_{tot}/K, we set

$$P_k = P_{\mathrm{c}} = \frac{T}{N}\frac{P_{\mathrm{tot}}}{K}. \tag{2.4}$$

Then $P_{\mathrm{c}}(N/T) = P_{\mathrm{tot}}/K$, and the received signal model can be rewritten as

$$\mathbf{y} = \sqrt{P_{\mathrm{c}}}\mathcal{B}(\mathbf{x})\mathbf{R}\mathbf{h} + \mathbf{w}, \tag{2.5}$$

where $\mathbf{R} = [\mathbf{r}_1, \ldots, \mathbf{r}_K] \in \mathbb{C}^{L\times K}$, $\tilde{\mathbf{h}} = [\tilde{h}_1, \ldots, \tilde{h}_K]^{\mathrm{T}} \sim \mathcal{CN}(\mathbf{0}, \mathbf{I}_K)$, $\mathbf{h} = \Sigma^{1/2}\tilde{\mathbf{h}} = [h_1, \ldots, h_K]^{\mathrm{T}}$, and $\mathbf{h} \sim \mathcal{CN}(\mathbf{0}, \Sigma)$ with $\Sigma = \mathrm{diag}(\sigma_1, \ldots, \sigma_K)$. Throughout this paper, the receiver is assumed to have perfect knowledge of the effective channel vector $\mathbf{h}_{\mathrm{eff}} = \mathbf{R}\mathbf{h}$ for coherent O-STBC combining. This assumption is used to derive the post-combining SNR and the corresponding performance expressions. By contrast, receiver-side estimation accuracy does not affect the probability law of the underlying effective channel gain. Under imperfect estimation, the post-combining SNR must additionally account for the resulting mismatch, which can, for example, be represented by an additive complex Gaussian error model [27].

2.2. Post-combining received SNR

Proposition 2.1 (Post-combining SNR of FD-STBC)**.** *Under the signal model in* (2.5)*, the output of the conventional O-STBC combiner can be written as*

$$\overline{\mathbf{y}} = \sqrt{P_{\mathrm{c}}}\|\mathbf{R}\mathbf{h}\|\mathbf{x} + \overline{\mathbf{w}}, \tag{2.6}$$

where $\overline{\mathbf{w}} \sim \mathcal{CN}(\mathbf{0}, N_0\mathbf{I}_N)$*. Consequently, if*

$$Z = \|\mathbf{R}\mathbf{h}\|^2 \tag{2.7}$$

and

$$\rho = \frac{P_{\mathrm{c}}}{N_0} = \frac{T}{N}\frac{P_{\mathrm{tot}}}{KN_0}, \tag{2.8}$$

then the instantaneous received SNR after decoding is

$$\gamma = \rho Z. \tag{2.9}$$

Proof. Define the effective channel vector $\mathbf{h}_{\mathrm{eff}} = \mathbf{R}\mathbf{h} \in \mathbb{C}^L$. Then (2.5) has the same algebraic form as a conventional O-STBC transmission with the effective channel vector $\mathbf{h}_{\mathrm{eff}}$. The orthogonality condition in (2.1) implies that the normalized O-STBC combiner diagonalizes the symbol vector and produces the scalar channel amplitude $\|\mathbf{h}_{\mathrm{eff}}\|$ for every decoded symbol. The normalization by $\|\mathbf{h}_{\mathrm{eff}}\|$ also preserves the AWGN covariance, so the post-combining noise remains $\mathcal{CN}(\mathbf{0}, N_0\mathbf{I}_N)$. Thus (2.6) follows. The conditional signal power per decoded symbol is $P_{\mathrm{c}}\|\mathbf{h}_{\mathrm{eff}}\|^2$, and the noise variance is N_0. Using $Z = \|\mathbf{h}_{\mathrm{eff}}\|^2 = \|\mathbf{R}\mathbf{h}\|^2$ and $\rho = P_{\mathrm{c}}/N_0$ gives (2.9). □

The following examples illustrate the post-combining model in Proposition 2.1 for two common O-STBC dimensions.

Example 2.2 (Full-rate O-STBC with $T = 2$, $N = 2$, and $L = 2$)**.** *For $T = N = L = 2$, the common codeword can be chosen as the Alamouti code*

$$\mathcal{B}^2_{2/2}(\mathbf{x}) = \begin{bmatrix} x_1 & x_2 \\ -x_2^* & x_1^* \end{bmatrix}, \qquad \mathbf{x} = [x_1, x_2]^{\mathrm{T}}. \tag{2.10}$$

Since $N = T = 2$, $P_{\mathrm{c}} = P_{\mathrm{tot}}/K$. After conjugating the second slot's received signal, the equivalent received vector is

$$\begin{bmatrix} y_1 \\ y_2^* \end{bmatrix} = \sqrt{P_{\mathrm{c}}}\begin{bmatrix} h_{\mathrm{eff},1} & h_{\mathrm{eff},2} \\ h_{\mathrm{eff},2}^* & -h_{\mathrm{eff},1}^* \end{bmatrix}\begin{bmatrix} x_1 \\ x_2 \end{bmatrix} + \begin{bmatrix} w_1 \\ w_2^* \end{bmatrix}. \tag{2.11}$$

The normalized Alamouti combiner yields

$$\overline{\mathbf{y}} = \frac{1}{||\mathbf{h}_{\text{eff}}||}\begin{bmatrix} h^*_{\text{eff},1} & h_{\text{eff},2} \\ h^*_{\text{eff},2} & -h_{\text{eff},1} \end{bmatrix}\begin{bmatrix} y_1 \\ y^*_2 \end{bmatrix} = \sqrt{P_\text{c}}||\mathbf{h}_{\text{eff}}||\mathbf{x} + \overline{\mathbf{w}} = \sqrt{P_\text{c}}||\mathbf{R}\mathbf{h}||\mathbf{x} + \overline{\mathbf{w}}, \tag{2.12}$$

where $\overline{\mathbf{w}} \sim \mathcal{CN}(\mathbf{0}, N_0\mathbf{I}_2)$*. Hence, both QAM symbols are decoded with the same effective gain* $Z = ||\mathbf{h}_{\text{eff}}||^2 = ||\mathbf{R}\mathbf{h}||^2$.

Example 2.3 (Rate-3/4 O-STBC with $T = 4$, $N = 3$, and $L = 3$)**.** *A rate-*3/4 *O-STBC codeword is*

$$\mathcal{B}^3_{3/4}(\mathbf{x}) = \begin{bmatrix} x_1 & x_2 & 0 \\ -x^*_2 & x^*_1 & x^*_3 \\ x_3 & 0 & x_2 \\ 0 & -x_3 & x_1 \end{bmatrix}, \qquad \mathbf{x} = [x_1, x_2, x_3]^{\text{T}}. \tag{2.13}$$

Here, $P_\text{c} = (4/3)(P_{\text{tot}}/K)$*, so the rate compensation keeps the actual time-averaged transmit power of each node equal to* P_{tot}/K*. After conjugating the second slot received signal, we have*

$$\begin{bmatrix} y_1 \\ y^*_2 \\ y_3 \\ y_4 \end{bmatrix} = \sqrt{P_\text{c}}\begin{bmatrix} h_{\text{eff},1} & h_{\text{eff},2} & 0 \\ h^*_{\text{eff},2} & -h^*_{\text{eff},1} & h^*_{\text{eff},3} \\ 0 & h_{\text{eff},3} & h_{\text{eff},1} \\ h_{\text{eff},3} & 0 & -h_{\text{eff},2} \end{bmatrix}\begin{bmatrix} x_1 \\ x_2 \\ x_3 \end{bmatrix} + \begin{bmatrix} w_1 \\ w^*_2 \\ w_3 \\ w_4 \end{bmatrix}. \tag{2.14}$$

Applying the conventional O-STBC combiner gives

$$\overline{\mathbf{y}} = \frac{1}{||\mathbf{h}_{\text{eff}}||}\begin{bmatrix} h_{\text{eff},1} & h_{\text{eff},2} & 0 \\ h^*_{\text{eff},2} & -h^*_{\text{eff},1} & h^*_{\text{eff},3} \\ 0 & h_{\text{eff},3} & h_{\text{eff},1} \\ h_{\text{eff},3} & 0 & -h_{\text{eff},2} \end{bmatrix}^{\text{H}}\begin{bmatrix} y_1 \\ y^*_2 \\ y_3 \\ y_4 \end{bmatrix} = \sqrt{P_\text{c}}||\mathbf{h}_{\text{eff}}||\mathbf{x} + \overline{\mathbf{w}}, \tag{2.15}$$

where $\overline{\mathbf{w}} \sim \mathcal{CN}(\mathbf{0}, N_0\mathbf{I}_3)$*. Thus, the rate-*3/4 *example has the same post-combining scalar gain form as the Alamouti example; only the number of decoded symbols and the deterministic rate compensation factor* T/N *differ.*

2.3. Problem statement

Proposition 2.1 shows that the performance of the considered FD-STBC system is governed by the scalar effective channel gain

$$Z = ||\mathbf{h}_{\text{eff}}||^2 = ||\mathbf{R}\mathbf{h}||^2. \tag{2.16}$$

Therefore, the mathematical problem studied in this paper is to characterize the exact unconditional distribution of Z when the columns of $\mathbf{R}$ are independent complex unit-hyperspherical vectors and $\mathbf{h} \sim \mathcal{CN}(\mathbf{0}, \Sigma)$. Once this distribution is known, key performance measures such as outage probability, BER, and diversity order can be computed by deterministic analytical formulas rather than by repeated Monte Carlo averaging over $\mathbf{R}$ and $\mathbf{h}$ for each parameter setting. The resulting analytical expressions also enable examination of how the system performance varies with the key parameters, thereby providing a basis for systematic parameter studies of FD-STBC systems with hyperspherical signatures [9, 10]. The main system and analysis parameters are summarized in Table 2.

Table 2. Summary of main parameters.

Symbol	Description
K	Number of distributed transmitters.
L	Number of virtual transmit dimensions; equivalently, the number of columns of the common O-STBC codeword ($L \geq 2$).
T	Number of channel uses occupied by one O-STBC codeword; equivalently, the number of rows of the common O-STBC codeword ($T \geq 2$).
N	Number of information symbols carried by one O-STBC codeword.
$\mathbf{r}_k$	Length-L random signature vector of transmitter k, with $\|\mathbf{r}_k\| = 1$.
$\mathbf{R}$	Signature matrix $[\mathbf{r}_1, \ldots, \mathbf{r}_K] \in \mathbb{C}^{L\times K}$.
h_k	Wireless channel coefficient from transmitter k to the receiver.
σ_k	Average channel power of transmitter k, including large-scale fading components.
Z	Effective post-combining channel gain $\|\mathbf{R}\mathbf{h}\|^2$.
P_{tot}	Total time-averaged network transmit power.
$P_{\text{c}} = (T/N)(P_{\text{tot}}/K)$	Common rate-compensated codeword-level power coefficient.
N_0	Complex noise variance at the receiver.
$\rho = P_{\text{c}}/N_0$	Rate-compensated per-node transmit SNR.
$\gamma = \rho Z$	Instantaneous received SNR after O-STBC combining.

3. Exact distribution of the effective channel gain

In this section, we derive the exact unconditional distribution of the effective channel gain Z. We first recall the conditional eigenvalue representation and then derive a more useful unconditional scale-mixture representation.

3.1. Conditional eigenvalue law

First, the effective channel gain can be written as a quadratic form

$$Z = \|\mathbf{R}\mathbf{h}\|^2 = \tilde{\mathbf{h}}^{\text{H}}\Sigma^{1/2}\mathbf{R}^{\text{H}}\mathbf{R}\Sigma^{1/2}\tilde{\mathbf{h}}. \tag{3.1}$$

This is a Hermitian quadratic form in a complex Gaussian vector, and the conditional eigenvalue representation below is consistent with the classical theory of quadratic forms in random variables [28]. Conditioned on $\mathbf{R}$, define $\mathbf{Q}_{\mathbf{R}} \triangleq \Sigma^{1/2}\mathbf{R}^{\text{H}}\mathbf{R}\Sigma^{1/2} \in \mathbb{C}^{K\times K}$. Then $\mathbf{Q}_{\mathbf{R}}$ is Hermitian positive semidefinite. Let $m = \min(K, L)$, and let $\lambda_1 = \lambda_1(\mathbf{R}), \ldots, \lambda_m = \lambda_m(\mathbf{R})$ be the nonzero eigenvalues of $\mathbf{Q}_{\mathbf{R}}$. For notational simplicity, we suppress their dependence on $\mathbf{R}$. Furthermore, let $\mathbf{U}\Lambda\mathbf{U}^{\text{H}}$ be the eigenvalue decomposition of $\mathbf{Q}_{\mathbf{R}}$, where $\mathbf{U}$ is the unitary matrix and $\Lambda = \text{diag}(\lambda_1, \ldots, \lambda_m, 0, \ldots, 0) \in \mathbb{R}_+^{K\times K}$ is the diagonal matrix of eigenvalues. Since $\mathbf{U}$ is unitary and $\tilde{\mathbf{h}} \sim \mathcal{CN}(\mathbf{0}, \mathbf{I}_K)$, we have $\bar{\mathbf{h}} = \mathbf{U}^{\text{H}}\tilde{\mathbf{h}} \sim \mathcal{CN}(\mathbf{0}, \mathbf{I}_K)$. Therefore, conditioned on $\mathbf{R}$, the random variable Z has the following distribution [9, 10]:

$$Z \mid \mathbf{R} \stackrel{d}{=} \sum_{i=1}^{m} \lambda_i |\bar{h}_i|^2 = \sum_{i=1}^{m} \lambda_i E_i, \qquad E_i \sim \text{Exp}(1), \tag{3.2}$$

where the E_i's are independent. Hence, the conditional Laplace transform of Z is

$$\mathcal{L}_{Z|\mathbf{R}}(s|\mathbf{R}) \triangleq \mathbb{E}[e^{-sZ}\,|\,\mathbf{R}] = \frac{1}{\det(\mathbf{I}_K + s\mathbf{Q}_{\mathbf{R}})} = \prod_{i=1}^{m} \frac{1}{1+s\lambda_i} \overset{(a)}{=} \sum_{i=1}^{m} \frac{\kappa_i}{1+s\lambda_i}, \tag{3.3}$$

where (a) is the partial fraction expansion, which is valid when the nonzero eigenvalues are distinct. For the random hyperspherical matrix considered here, repeated nonzero eigenvalues occur only on a lower-dimensional subset and hence do not affect the unconditional distribution; moreover, the scale-mixture derivation in the next subsection does not rely on this partial fraction representation. Taking the inverse Laplace transform then gives the conditional PDF in the hypoexponential form

$$f_{Z|\mathbf{R}}(z|\mathbf{R}) = \sum_{i=1}^{m} \frac{\kappa_i}{\lambda_i} \exp\left(-\frac{z}{\lambda_i}\right),\ z \geq 0, \quad \text{where } \kappa_i = \prod_{\substack{j=1\\ j\neq i}}^{m} \frac{\lambda_i}{\lambda_i - \lambda_j}. \tag{3.4}$$

Although the conditional eigenvalue representation is exact, obtaining the unconditional PDF by averaging $f_Z(z) = \mathbb{E}_{\mathbf{R}}[f_{Z|\mathbf{R}}(z|\mathbf{R})]$ is nontrivial because it would require characterizing the joint distribution of the eigenvalues induced by the hyperspherical columns of $\mathbf{R}$.

3.2. Gamma–beta scale-mixture representation

We next derive a representation that bypasses the eigenvalue distribution. Instead of characterizing the eigenvalues of the random Gram matrix induced by hyperspherical columns, we analyze the effective channel vector itself as a sum of independent isotropic random vectors, $\mathbf{R}\mathbf{h} = \sum_{k=1}^{K} h_k \mathbf{r}_k$. This leads to an exact gamma–beta scale-mixture representation. For clarity, the principal random variables used in the gamma–beta scale-mixture representation are summarized in Table 3.

Table 3. Principal random variables in the gamma–beta scale-mixture representation.

Symbol	Description
Z	Effective post-combining channel gain whose distribution is characterized
U_k	$\mathrm{Beta}(1, L-1)$ projection variable associated with $\mathbf{r}_k$; mutually independent over k
$X_k = \sigma_k U_k$	Weighted beta random variable supported on $[0, \sigma_k]$
$A = \sum_{k=1}^{K} X_k$	Weighted beta sum serving as the random scale
G_L	Unit-rate $\mathrm{Gamma}(L, 1)$ random variable independent of A

Lemma 3.1. *Let $\mathbf{r}$ be uniformly distributed on the complex unit hypersphere in $\mathbb{C}^L$, and let $\mathbf{u} \in \mathbb{C}^L$ be any deterministic unit vector. Then*

$$|\mathbf{u}^{\mathrm{H}}\mathbf{r}|^2 \sim \mathrm{Beta}(1, L-1). \tag{3.5}$$

Proof. By the rotational invariance of the uniform distribution on the complex unit hypersphere, $|\mathbf{u}^{\mathrm{H}}\mathbf{r}|^2$ has the same distribution as $|r_1|^2$, the squared magnitude of the first coordinate of $\mathbf{r}$. Let $\mathbf{g} \sim \mathcal{CN}(\mathbf{0}, \mathbf{I}_L)$. Then $\mathbf{g}/\|\mathbf{g}\|$ is uniformly distributed on the complex unit hypersphere, and hence

$$|r_1|^2 \overset{d}{=} \frac{|g_1|^2}{\sum_{\ell=1}^{L} |g_\ell|^2}. \tag{3.6}$$

Since $|g_1|^2, \dots, |g_L|^2$ are independent unit-mean exponential or, equivalently, Gamma$(1, 1)$ random variables, the normalized vector

$$\left[\frac{|g_1|^2}{\sum_{\ell=1}^{L} |g_\ell|^2}, \dots, \frac{|g_L|^2}{\sum_{\ell=1}^{L} |g_\ell|^2}\right] \tag{3.7}$$

has a Dirichlet$(1, \dots, 1)$ distribution. Therefore, the first component of this normalized vector has a Beta$(1, L - 1)$ distribution [3]. □

Theorem 3.2 (Exact scale-mixture law)**.** *Consider*

$$Z = \left\| \sum_{k=1}^{K} h_k \mathbf{r}_k \right\|^2. \tag{3.8}$$

Define

$$A = \sum_{k=1}^{K} \sigma_k U_k, \qquad U_k \sim \text{Beta}(1, L - 1), \tag{3.9}$$

where $U_1, \dots, U_K$ are mutually independent, and let

$$G_L \sim \text{Gamma}(L, 1), \tag{3.10}$$

independent of A, with the PDF $f_{G_L}(x) = x^{L-1}e^{-x}/\Gamma(L)$ for $x \ge 0$. Then

$$Z \stackrel{d}{=} AG_L. \tag{3.11}$$

Proof. Define the effective channel vector

$$\mathbf{h}_{\text{eff}} = \sum_{k=1}^{K} h_k \mathbf{r}_k \in \mathbb{C}^L. \tag{3.12}$$

For an arbitrary test vector $\boldsymbol{\omega} \in \mathbb{C}^L$, consider the real characteristic function

$$\varphi_{\mathbf{h}_{\text{eff}}}(\boldsymbol{\omega}) = \mathbb{E}\left[\exp\left(j\,\text{Re}\{\boldsymbol{\omega}^{\text{H}} \mathbf{h}_{\text{eff}}\}\right)\right]. \tag{3.13}$$

Conditioned on $\mathbf{r}_k$, the scalar $\boldsymbol{\omega}^{\text{H}} h_k \mathbf{r}_k$ is a complex Gaussian random variable with the variance $\sigma_k |\boldsymbol{\omega}^{\text{H}} \mathbf{r}_k|^2$. Since the real part of a $\mathcal{CN}(0, \sigma)$ random variable has the variance $\sigma/2$, we obtain

$$\mathbb{E}\left[\exp\left(j\,\text{Re}\{\boldsymbol{\omega}^{\text{H}} h_k \mathbf{r}_k\}\right) \middle| \mathbf{r}_k\right] = \exp\left(-\frac{\sigma_k |\boldsymbol{\omega}^{\text{H}} \mathbf{r}_k|^2}{4}\right). \tag{3.14}$$

For $\boldsymbol{\omega} \neq \mathbf{0}$, set $\mathbf{u} = \boldsymbol{\omega}/\|\boldsymbol{\omega}\|$. Then $|\boldsymbol{\omega}^{\text{H}} \mathbf{r}_k|^2 = \|\boldsymbol{\omega}\|^2 |\mathbf{u}^{\text{H}} \mathbf{r}_k|^2$, and, by Lemma 3.1, $|\mathbf{u}^{\text{H}} \mathbf{r}_k|^2 \sim \text{Beta}(1, L - 1)$. The case $\boldsymbol{\omega} = \mathbf{0}$ is immediate. Hence, the replacement

$$|\boldsymbol{\omega}^{\text{H}} \mathbf{r}_k|^2 \stackrel{d}{=} \|\boldsymbol{\omega}\|^2 U_k, \tag{3.15}$$

is valid for $U_k \sim \text{Beta}(1, L - 1)$. Since the signature vectors $\mathbf{r}_1, \dots, \mathbf{r}_K$ are mutually independent, the corresponding variables $U_1, \dots, U_K$ can be taken to be mutually independent. Using the independence, we obtain

$$\varphi_{\mathbf{h}_{\text{eff}}}(\boldsymbol{\omega}) = \prod_{k=1}^{K} \mathbb{E}_{\mathbf{r}_k}\left[\exp\left(-\frac{\sigma_k |\boldsymbol{\omega}^{\text{H}} \mathbf{r}_k|^2}{4}\right)\right] = \prod_{k=1}^{K} \mathbb{E}_{U_k}\left[\exp\left(-\frac{\sigma_k \|\boldsymbol{\omega}\|^2 U_k}{4}\right)\right] = \mathbb{E}_A\left[\exp\left(-\frac{A\|\boldsymbol{\omega}\|^2}{4}\right)\right]. \tag{3.16}$$

On the other hand, if $\mathbf{g} \sim \mathcal{CN}(\mathbf{0}, \mathbf{I}_L)$ is independent of A, then the characteristic function of $\sqrt{A}\mathbf{g}$ is exactly the right-hand side of (3.16). Therefore $\mathbf{h}_{\text{eff}} \overset{d}{=} \sqrt{A}\mathbf{g}$. More precisely, construct A and $\mathbf{g}$ on a product probability space so that they are jointly independent; the two characteristic functions then coincide for every $\boldsymbol{\omega}$, and the Lévy continuity theorem yields the distributional equality. Taking squared Euclidean norms gives

$$Z = \|\mathbf{h}_{\text{eff}}\|^2 \overset{d}{=} A\|\mathbf{g}\|^2. \tag{3.17}$$

Since $\|\mathbf{g}\|^2 \sim \text{Gamma}(L, 1)$, we may identify $\|\mathbf{g}\|^2$ with G_L. Therefore, the result of (3.11) follows. □

Intuitively, the gamma–beta scale-mixture law separates the directional randomness of the hyperspherical signatures from the radial randomness of an isotropic complex Gaussian vector. The squared directional projections produce the independent beta variables U_k, whose weighted sum $A = \sum_{k=1}^{K} \sigma_k U_k$ forms the random scale, while the Gaussian radial energy gives $G_L = \|\mathbf{g}\|^2 \sim \text{Gamma}(L, 1)$. Thus, the effective channel gain naturally takes the product form $Z \overset{d}{=} AG_L$.

Corollary 3.3 (Large-network limit and centralized O-STBC equivalence)**.** *Suppose equal average channel powers, $\sigma_k = \sigma$ for all $k \in \mathcal{K}$.* For each K, let Z be defined as in* (3.8)*. Then, for a fixed L, as $K \to \infty$,*

$$\frac{L}{K\sigma} Z \xrightarrow{d} G_L, \qquad G_L \sim \text{Gamma}(L, 1). \tag{3.18}$$

Under the rate-compensated SNR convention in (2.8)*, we have*

$$\gamma = \rho Z, \qquad \rho = \frac{T}{N} \frac{P_{\text{tot}}}{KN_0}. \tag{3.19}$$

Then

$$\gamma \xrightarrow{d} \frac{T}{N} \frac{P_{\text{tot}}}{N_0} \frac{\sigma}{L} G_L. \tag{3.20}$$

Thus, the post-combining SNR of FD-STBC converges to the scaled Erlang law associated with the corresponding centralized O-STBC system. This provides a distribution-level verification of the observation in [9] that R-STC approaches centralized O-STBC as the number of transmitters increases. In contrast to the central limit theorem (CLT)-based effective channel equivalence in [9, Theorem 4], the present result follows directly from the exact finite K gamma–beta scale-mixture law and explicitly identifies the limiting normalized gain and SNR distributions for complex hyperspherical signatures.

Proof. By Theorem 3.2

$$Z \overset{d}{=} AG_L, \qquad A = \sigma \sum_{k=1}^{K} U_k, \tag{3.21}$$

where $U_1, \ldots, U_K$ are i.i.d. Beta$(1, L-1)$ random variables that are independent of G_L. Since $\mathbb{E}[U_k] = 1/L$, the strong law of large numbers gives

$$\frac{A}{K\sigma} = \frac{1}{K} \sum_{k=1}^{K} U_k \xrightarrow{\text{a.s.}} \frac{1}{L}. \tag{3.22}$$

Slutsky's theorem then yields (3.18) [29, Ch. 2]. Finally, using $\gamma = \rho Z$ with $\rho = (T/N)P_{\text{tot}}/(KN_0)$ gives (3.20). □

*This assumption is reasonable when the cooperating nodes are clustered within a region whose diameter is small relative to their distance to the receiver, so the large-scale fading terms are approximately identical; this is consistent with the system models considered in [8, 9].

3.3. PDF and CDF of the effective channel gain

Let $f_A(a)$ denote the PDF of A in (3.9). Since $0 \le A \le \sum_{k=1}^{K} \sigma_k$, Theorem 3.2 gives the following integral forms for the exact PDF and CDF of Z.

Corollary 3.4 (Exact PDF and CDF)**.** *For $z > 0$, the PDF of Z is*

$$f_Z(z) = \frac{z^{L-1}}{\Gamma(L)} \int_0^{\sum_{k=1}^{K} \sigma_k} \frac{1}{a^L} \exp\left(-\frac{z}{a}\right) f_A(a) da. \tag{3.23}$$

For $z \ge 0$, the corresponding CDF is

$$F_Z(z) = 1 - \int_0^{\sum_{k=1}^{K} \sigma_k} \exp\left(-\frac{z}{a}\right) \sum_{n=0}^{L-1} \frac{1}{n!} \left(\frac{z}{a}\right)^n f_A(a) da. \tag{3.24}$$

Proof. Conditioned on $A = a$, the random variable $Z = aG_L$ has the PDF

$$f_{Z|A}(z|a) = \frac{z^{L-1}}{\Gamma(L) a^L} \exp\left(-\frac{z}{a}\right), \qquad z > 0.$$

Averaging this conditional PDF over A yields the PDF (3.23). For an integer $L \ge 2$, the conditional CDF is

$$F_{Z|A}(z|a) = 1 - \exp\left(-\frac{z}{a}\right) \sum_{n=0}^{L-1} \frac{1}{n!} \left(\frac{z}{a}\right)^n, \qquad z \ge 0.$$

Averaging this conditional CDF over A gives (3.24). □

The integral forms above are useful for interpretation but the distribution can be written without any unevaluated convolution. Let $\mathcal{K} = \{1, \ldots, K\}$ and $\sigma_{\text{tot}} = \sum_{k=1}^{K} \sigma_k$. For a subset $\mathcal{S} \subseteq \mathcal{K}$, let $\sigma_{\mathcal{S}} = \sum_{k \in \mathcal{S}} \sigma_k$ and $\sigma_\varnothing = 0$. For a multi-index $\mathbf{q} = (q_1, \ldots, q_K)$, write its total order as $|\mathbf{q}| = \sum_{k=1}^{K} q_k$. For each $\mathcal{S}$ and $\mathbf{q}$, define $\mathcal{M}(\mathcal{S}, \mathbf{q}) = \{\mathbf{m}_{\mathcal{S}} = (m_k)_{k \in \mathcal{S}} : 0 \le m_k \le q_k,\ k \in \mathcal{S}\}$ with $|\mathbf{m}_{\mathcal{S}}| = \sum_{k \in \mathcal{S}} m_k$. For $\mathcal{S} = \varnothing$, the inner sum over $\mathcal{M}(\varnothing, \mathbf{q})$ contains one empty term and $|\mathbf{m}_\varnothing| = 0$. Finally, define

$$p(\mathbf{q}, \mathcal{S}, \mathbf{m}_{\mathcal{S}}) = K + |\mathbf{q}| - |\mathbf{m}_{\mathcal{S}}| - 1, \tag{3.25}$$

which is a non-negative integer because $|\mathbf{m}_{\mathcal{S}}| \le |\mathbf{q}|$.

The density of A is the K-fold convolution of compactly supported polynomial densities. The following theorem gives this convolution explicitly as a finite sum of shifted truncated polynomials. The integer q_k is produced by expanding the polynomial density of $X_k = \sigma_k U_k$. The subset $\mathcal{S}$ is an algebraic index set used in the Laplace domain expansion and does not represent a subset of active transmitters. It records which indices select the delayed exponential factor $e^{-s\sigma_k}$ in the Laplace domain, and the integer m_k arises from the finite incomplete-gamma expansion of $\int_0^{\sigma_k} x^{q_k} e^{-sx} dx$. Thus, the formula is a closed-form convolution of K compactly supported beta-type densities.

Theorem 3.5 (Fully expanded density of A)**.** *For $L \ge 2$, $\sigma_k > 0$ for all $k \in \mathcal{K}$, and $0 < a < \sigma_{\text{tot}}$, the density of $A = \sum_{k=1}^{K} \sigma_k U_k$ is*

$$f_A(a) = \sum_{\mathbf{q} \in \{0,\ldots,L-2\}^K} \sum_{\mathcal{S} \subseteq \mathcal{K}} \sum_{\mathbf{m}_{\mathcal{S}} \in \mathcal{M}(\mathcal{S}, \mathbf{q})} \Omega(\mathbf{q}, \mathcal{S}, \mathbf{m}_{\mathcal{S}}) \, (a - \sigma_{\mathcal{S}})_+^{p(\mathbf{q}, \mathcal{S}, \mathbf{m}_{\mathcal{S}})}, \tag{3.26}$$

where $x_+ = \max(x, 0)$ *and*

$$\Omega(\mathbf{q}, \mathcal{S}, \mathbf{m}_{\mathcal{S}}) = \frac{(L-1)^K (-1)^{|\mathcal{S}|+|\mathbf{q}|}}{\Gamma(K + |\mathbf{q}| - |\mathbf{m}_{\mathcal{S}}|) \prod_{k=1}^{K} \sigma_k^{L-1}} \prod_{k=1}^{K} \left[\binom{L-2}{q_k} \sigma_k^{L-2-q_k} q_k! \right] \prod_{k \in \mathcal{S}} \frac{\sigma_k^{m_k}}{m_k!}. \tag{3.27}$$

The density is zero outside $[0, \sigma_{\mathrm{tot}}]$.

Proof. The density of $X_k = \sigma_k U_k$ is

$$f_{X_k}(x) = \frac{L-1}{\sigma_k^{L-1}} (\sigma_k - x)^{L-2}, \qquad 0 < x < \sigma_k. \tag{3.28}$$

Expanding the polynomial and taking the Laplace transform gives

$$\begin{aligned} \mathcal{L}_{X_k}(s) &= \frac{L-1}{\sigma_k^{L-1}} \sum_{q_k=0}^{L-2} (-1)^{q_k} \binom{L-2}{q_k} \sigma_k^{L-2-q_k} \int_0^{\sigma_k} x^{q_k} e^{-sx} dx \\ &= \frac{L-1}{\sigma_k^{L-1}} \sum_{q_k=0}^{L-2} (-1)^{q_k} \binom{L-2}{q_k} \sigma_k^{L-2-q_k} q_k! s^{-(q_k+1)} \left[1 - e^{-s\sigma_k} \sum_{m_k=0}^{q_k} \frac{(s\sigma_k)^{m_k}}{m_k!} \right]. \end{aligned} \tag{3.29}$$

Since $A = \sum_k X_k$, the Laplace transform of A is the product of the K transforms. For a fixed $\mathbf{q}$, multiplying the square brackets above gives one algebraic choice for each index k: Either the non-shifted term 1, or the shifted finite sum

$$- e^{-s\sigma_k} \sum_{m_k=0}^{q_k} \frac{(s\sigma_k)^{m_k}}{m_k!}. \tag{3.30}$$

If the shifted term is selected for exactly the indices in $\mathcal{S}$, the exponential factors combine into $e^{-s\sigma_{\mathcal{S}}}$, the sign becomes $(-1)^{|\mathcal{S}|}$, and the powers of s are reduced by $|\mathbf{m}_{\mathcal{S}}|$. Hence, every expanded product term has the form

$$e^{-s\sigma_{\mathcal{S}}} s^{-(K+|\mathbf{q}|-|\mathbf{m}_{\mathcal{S}}|)}. \tag{3.31}$$

All remaining factors that do not depend on s are collected in $\Omega(\mathbf{q}, \mathcal{S}, \mathbf{m}_{\mathcal{S}})$. Applying the elementary time-shift inverse Laplace transform [30]

$$\mathcal{L}^{-1} \left\{ e^{-s\sigma_{\mathcal{S}}} s^{-(K+|\mathbf{q}|-|\mathbf{m}_{\mathcal{S}}|)} \right\} = \frac{(a - \sigma_{\mathcal{S}})_+^{K+|\mathbf{q}|-|\mathbf{m}_{\mathcal{S}}|-1}}{\Gamma(K + |\mathbf{q}| - |\mathbf{m}_{\mathcal{S}}|)}, \tag{3.32}$$

where $K + |\mathbf{q}| - |\mathbf{m}_{\mathcal{S}}| > 0$ holds automatically because $|\mathbf{m}_{\mathcal{S}}| \le |\mathbf{q}|$, gives (3.26). □

The fully expanded expression in (3.26) is a finite sum for every fixed K and L. This finite-sum representation provides a deterministic computational basis for evaluating the derived PDF, CDF, outage probability, and BER expressions. The following closed-form expressions for the PDF and CDF of Z are obtained by substituting (3.26) into (3.23) and (3.24). For $0 \le x \le y$, define

$$\mathcal{G}_\eta(x, y; z) = \int_x^y a^\eta \exp\left(-\frac{z}{a} \right) da, \tag{3.33}$$

with the convention $\mathcal{G}_\eta(x, x; z) = 0$. For $x < y$, this can be evaluated using the upper incomplete gamma function $\Gamma(s, x)$ [31, Ch. 8] as

$$\mathcal{G}_\eta(x, y; z) = z^{\eta+1}\left[\Gamma\left(-\eta - 1, \frac{z}{y}\right) - \Gamma\left(-\eta - 1, \frac{z}{x}\right)\right], \tag{3.34}$$

where $z/0$ is interpreted as $+\infty$.

Corollary 3.6 (Fully expanded PDF and CDF of Z)**.** *For $z > 0$,*

$$f_Z(z) = \frac{z^{L-1}}{\Gamma(L)} \sum_{\mathbf{q}} \sum_{\mathcal{S}} \sum_{\mathbf{m}_\mathcal{S}} \sum_{n=0}^{p(\mathbf{q},\mathcal{S},\mathbf{m}_\mathcal{S})} \Omega(\mathbf{q}, \mathcal{S}, \mathbf{m}_\mathcal{S}) \binom{p(\mathbf{q}, \mathcal{S}, \mathbf{m}_\mathcal{S})}{n} (-\sigma_\mathcal{S})^{p(\mathbf{q},\mathcal{S},\mathbf{m}_\mathcal{S})-n} \mathcal{G}_{n-L}(\sigma_\mathcal{S}, \sigma_{\mathrm{tot}}; z), \tag{3.35}$$

and

$$F_Z(z) = 1 - \sum_{r=0}^{L-1} \frac{z^r}{r!} \sum_{\mathbf{q}} \sum_{\mathcal{S}} \sum_{\mathbf{m}_\mathcal{S}} \sum_{n=0}^{p(\mathbf{q},\mathcal{S},\mathbf{m}_\mathcal{S})} \Omega(\mathbf{q}, \mathcal{S}, \mathbf{m}_\mathcal{S}) \binom{p(\mathbf{q}, \mathcal{S}, \mathbf{m}_\mathcal{S})}{n} (-\sigma_\mathcal{S})^{p(\mathbf{q},\mathcal{S},\mathbf{m}_\mathcal{S})-n} \mathcal{G}_{n-r}(\sigma_\mathcal{S}, \sigma_{\mathrm{tot}}; z), \tag{3.36}$$

where $p(\mathbf{q}, \mathcal{S}, \mathbf{m}_\mathcal{S})$ is defined in (3.25)*. In* (3.35) *and* (3.36)*, the sums over $\mathbf{q}$, $\mathcal{S}$, and $\mathbf{m}_\mathcal{S}$ have the same ranges as in* (3.26)*. The expanded CDF expression is evaluated for $z > 0$, with $F_Z(0) = 0$ by continuity.*

Corollary 3.7 (Laplace transform of Z)**.** *For $s \geq 0$,*

$$\mathcal{L}_Z(s) = \mathbb{E}[e^{-sZ}] = \mathbb{E}_A[(1 + sA)^{-L}]. \tag{3.37}$$

As a supplementary transform-domain characterization, the corresponding Lauricella series representation is

$$\mathcal{L}_Z(s) = F_A^{(K)}\left(L; \underbrace{1, \ldots, 1}_{K}; \underbrace{L, \ldots, L}_{K}; -s\sigma_1, \ldots, -s\sigma_K\right), \tag{3.38}$$

where $F_A^{(K)}(\cdot)$ denotes Lauricella's hypergeometric function of Type A [32, 33]. The defining series in (3.38) *converges when $\sum_{k=1}^{K} |s\sigma_k| < 1$; outside this convergence domain, the expression is understood by analytic continuation of the Laplace transform in* (3.37)*.*

Proof. By Theorem 3.2, conditioned on $A = a$, Z has the same distribution as aG_L, and hence

$$\mathbb{E}[e^{-sZ} | A = a] = (1 + sa)^{-L}. \tag{3.39}$$

Averaging over A gives (3.37).

For (3.38), write $(1 + sA)^{-L} = (1 + s\sum_{k=1}^{K} \sigma_k U_k)^{-L}$. Expanding this term into its multinomial series gives

$$\left(1 + s\sum_{k=1}^{K} \sigma_k U_k\right)^{-L} = \sum_{n_1,\ldots,n_K \geq 0} \frac{(L)_{|\mathbf{n}|}}{n_1! \cdots n_K!} \prod_{k=1}^{K} (-s\sigma_k U_k)^{n_k}, \tag{3.40}$$

where $\mathbf{n} = (n_1, \ldots, n_K)$ and $|\mathbf{n}| = \sum_{k=1}^{K} n_k$. Taking expectation and using the independence of the U_k's together with $\mathbb{E}[U_k^n] = (1)_n/(L)_n$, $U_k \sim \mathrm{Beta}(1, L - 1)$, gives (3.38), where $(x)_n$ denotes the Pochhammer symbol. The equality in (3.38) follows from the defining series in its convergence domain and elsewhere by analytic continuation. □

As another consequence of the scale-mixture representation, the moments of Z admit compact closed-form expressions.

Corollary 3.8 (Moments of Z)**.** *For every positive integer n, we have*

$$\mathbb{E}[Z^n] = (L)_n n! \sum_{\substack{\boldsymbol{\nu}\in\mathbb{Z}_+^K \\ |\boldsymbol{\nu}|=n}} \prod_{k=1}^{K} \frac{\sigma_k^{\nu_k}}{(L)_{\nu_k}}, \tag{3.41}$$

where $|\boldsymbol{\nu}| = \sum_{k=1}^{K} \nu_k$. In particular, the mean and variance are

$$\mathbb{E}[Z] = \sigma_{\mathrm{tot}}, \qquad \mathrm{Var}[Z] = \sum_{k=1}^{K} \sigma_k^2 + \frac{1}{L} \sum_{k\neq j} \sigma_k \sigma_j, \tag{3.42}$$

where $\sum_{k\neq j}$ is taken over all ordered index pairs with $k \neq j$, and hence $\sum_{k\neq j} \sigma_k\sigma_j = \sigma_{\mathrm{tot}}^2 - \sum_{k=1}^{K} \sigma_k^2$. Thus the mean equals the total average channel power σ_{tot}, and the variance splits into a self term $\sum_k \sigma_k^2$ and a cross-signature term that decays as $1/L$; the latter reflects the expected squared inner product $\mathbb{E}[|\mathbf{r}_i^{\mathrm{H}}\mathbf{r}_j|^2] = 1/L$ for $i \neq j$, which vanishes as the underlying O-STBC dimension L increases.

Proof. By Theorem 3.2, $Z \overset{d}{=} AG_L$, where A and G_L are independent. Therefore, $\mathbb{E}[Z^n] = \mathbb{E}[A^n]\,\mathbb{E}[G_L^n]$. For $G_L \sim \mathrm{Gamma}(L, 1)$, we have $\mathbb{E}[G_L^n] = (L)_n$. Moreover, the independence of the U_k's and the identity

$$\mathbb{E}[U_k^r] = \frac{(1)_r}{(L)_r} = \frac{r!}{(L)_r}, \qquad r \geq 0, \tag{3.43}$$

for $U_k \sim \mathrm{Beta}(1, L-1)$, together with the multinomial expansion of $A^n = \left(\sum_{k=1}^{K} \sigma_k U_k\right)^n$, give

$$\mathbb{E}[A^n] = n! \sum_{\substack{\boldsymbol{\nu}\in\mathbb{Z}_+^K \\ |\boldsymbol{\nu}|=n}} \prod_{k=1}^{K} \frac{\sigma_k^{\nu_k}}{(L)_{\nu_k}}. \tag{3.44}$$

Combining this result with $\mathbb{E}[G_L^n] = (L)_n$ yields (3.41). Setting $n = 1$ gives $\mathbb{E}[A] = \sigma_{\mathrm{tot}}/L$, and hence $\mathbb{E}[Z] = \sigma_{\mathrm{tot}}$. For $n = 2$, (3.44) gives

$$\mathbb{E}[A^2] = \frac{2}{L(L+1)} \sum_{k=1}^{K} \sigma_k^2 + \frac{1}{L^2} \sum_{k\neq j} \sigma_k \sigma_j. \tag{3.45}$$

Using $\mathbb{E}[G_L^2] = (L)_2 = L(L+1)$, we obtain

$$\mathbb{E}[Z^2] = 2 \sum_{k=1}^{K} \sigma_k^2 + \frac{L+1}{L} \sum_{k\neq j} \sigma_k \sigma_j. \tag{3.46}$$

Subtracting $\mathbb{E}[Z]^2 = \sigma_{\mathrm{tot}}^2 = \sum_{k=1}^{K} \sigma_k^2 + \sum_{k\neq j} \sigma_k\sigma_j$ yields the variance in (3.42). □

3.4. Computational cost of the finite-sum representations

Although the expressions in Theorem 3.5 and Corollary 3.6 are finite for every fixed K and L, the number of terms grows rapidly with K and L. The following proposition quantifies this growth.

Proposition 3.9 (Term counts for the finite-sum representations)**.** *Let $N_{\mathrm{base}}(K, L)$ denote the number of $(\mathbf{q}, \mathcal{S}, \mathbf{m}_{\mathcal{S}})$-indexed terms in the fully expanded density of A in* (3.26)*. Then*

$$N_{\mathrm{base}}(K, L) = \left[\frac{(L-1)(L+2)}{2}\right]^K. \tag{3.47}$$

Consequently, the expanded PDF and CDF of Z in (3.35) *and* (3.36) *contain at most $K(L-1)N_{\mathrm{base}}(K, L)$ and $LK(L-1)N_{\mathrm{base}}(K, L)$ terms, respectively.*

Proof. For a fixed index k and $q_k \in \{0, \ldots, L-2\}$, the expansion contains one nonshifted choice corresponding to $k \notin \mathcal{S}$, and $q_k + 1$ shifted choices corresponding to $k \in \mathcal{S}$ and $m_k = 0, \ldots, q_k$. Hence, summing over $q_k = 0, \ldots, L-2$, the total number of choices contributed by index k is

$$\sum_{q=0}^{L-2} [1 + (q+1)] = \frac{(L-1)(L+2)}{2}. \tag{3.48}$$

Because the choices factor across the K indices, their product gives $N_{\mathrm{base}}(K, L)$. In (3.35), the index n has $p(\mathbf{q}, \mathcal{S}, \mathbf{m}_{\mathcal{S}}) + 1 = K + |\mathbf{q}| - |\mathbf{m}_{\mathcal{S}}| \le K(L-1)$ values, where the inequality follows from $|\mathbf{q}| \le K(L-2)$ and $|\mathbf{m}_{\mathcal{S}}| \ge 0$, while (3.36) also contains the L values of the index r. The stated upper bounds therefore follow. □

Thus, for a fixed L, $N_{\mathrm{base}}(K, L)$ grows exponentially with K, whereas for a fixed K, it grows on the order of L^{2K}. The direct finite-sum expressions are therefore most suitable for exact deterministic evaluation at small and moderate values of K and L, while their tractability deteriorates rapidly as either K or L grows.

Despite these computational limitations, the regime of small and moderate K and L remains practically meaningful for the FD-STBC application considered here. Increasing K enlarges the cooperating group and can increase the associated synchronization, group-formation, and scheduling burdens. Moreover, as shown later in Corollary 4.1, the diversity order is $\min(K, L)$, so increasing K beyond L does not provide an additional diversity order gain. Increasing L can also incur a coding rate reduction for higher-dimensional complex O-STBCs. For example, the $L = 2$ Alamouti code is full rate, whereas the $L = 3$ O-STBC in Example 2.3 has the rate $3/4$. More generally, the constructions in [26] have the rate $(k+1)/(2k)$ for $2k-1$ or $2k$ transmission dimensions. These considerations make small and moderate K and L a natural regime for direct finite-sum evaluation.

For larger values of K and L, the integral representations in (3.23) and (3.24) can provide a more scalable numerical route, but only if f_A is evaluated without enumerating the same finite expansion. For example, f_A can be approximated on a grid by recursive or fast Fourier transform (FFT)-based convolution of the K compactly supported summand densities, followed by one-dimensional quadrature of the mixture integrals. In contrast, evaluating the fully expanded f_A at every quadrature node retains the same combinatorial term count.

4. Applications to outage probability and BER analysis

This section applies the exact distribution of Z derived in Section 3 to characterize the outage probability, diversity order, and BER of FD-STBC with hyperspherical signatures. Since the outage probability follows directly from the CDF of Z, it is treated first. The resulting high-SNR asymptotic outage expansion is then used to derive the diversity order. Finally, the BER expression is obtained by averaging the conditional QAM error probability over Z.

4.1. Outage probability

The outage probability is the probability that the instantaneous received SNR falls below a target threshold $\gamma_{\text{th}} > 0$. For a rate-N/T O-STBC, the equivalent scalar channel gain yields the instantaneous spectral efficiency

$$R(\gamma) = \frac{N}{T}\log_2(1+\gamma) \tag{4.1}$$

per channel use. If R_0 denotes the target spectral efficiency per channel use, the outage event $R(\gamma) < R_0$ is equivalent to $\gamma < \gamma_{\text{th}}$, where $\gamma_{\text{th}} = 2^{(T/N)R_0} - 1$. If the target rate R_0 is instead measured per decoded O-STBC information symbol, then the corresponding threshold is $\gamma_{\text{th}} = 2^{R_0} - 1$. In the following, γ_{th} is treated as a prescribed SNR threshold. Since the SNR convention in (2.9) gives $\gamma = \rho Z$, the outage probability is directly derived from the CDF of Z as follows:

$$P_{\text{out}}(\gamma_{\text{th}}) = \Pr\{\gamma < \gamma_{\text{th}}\} = F_Z\left(\frac{\gamma_{\text{th}}}{\rho}\right). \tag{4.2}$$

Substituting the fully expanded CDF in (3.36) and using the argument γ_{th}/ρ directly, we obtain

$$P_{\text{out}}(\gamma_{\text{th}}) = 1 - \sum_{r=0}^{L-1}\frac{1}{r!}\left(\frac{\gamma_{\text{th}}}{\rho}\right)^{r}\sum_{\mathbf{q},\mathcal{S},\mathbf{m}_{\mathcal{S}},n}\Omega(\mathbf{q},\mathcal{S},\mathbf{m}_{\mathcal{S}})\binom{p(\mathbf{q},\mathcal{S},\mathbf{m}_{\mathcal{S}})}{n}(-\sigma_{\mathcal{S}})^{p(\mathbf{q},\mathcal{S},\mathbf{m}_{\mathcal{S}})-n}\mathcal{G}_{n-r}\left(\sigma_{\mathcal{S}},\sigma_{\text{tot}};\frac{\gamma_{\text{th}}}{\rho}\right). \tag{4.3}$$

The summation ranges of $\mathbf{q}$, $\mathcal{S}$, $\mathbf{m}_{\mathcal{S}}$, and n are the same as those in (3.36).

4.1.1. Asymptotic outage probability and diversity order

In communication theory, the diversity order has the physical interpretation of the number of equivalent independent fading branches that contribute to the reliability gain. One way to define it is through the high-SNR decay exponent of the outage probability. Specifically, for a fixed outage threshold γ_{th}, the exact outage expression in (4.2) gives $P_{\text{out}}(\gamma_{\text{th}}) = F_Z(\gamma_{\text{th}}/\rho)$. Hence, as $\rho \to \infty$, the argument γ_{th}/ρ approaches zero, and the high-SNR outage behavior is determined by the near-origin behavior of the CDF $F_Z(z)$. Therefore, the small-z expansion of $F_Z(z)$ yields the asymptotic outage probability and the corresponding diversity order.

Corollary 4.1 (Asymptotic outage probability and diversity order)**.** *For a fixed outage threshold* $\gamma_{\text{th}} > 0$*, define*

$$c_A = \frac{(L-1)^K}{(K-1)!\prod_{k=1}^{K}\sigma_k}. \tag{4.4}$$

For $K > L$, also define the finite negative moment

$$\mu_{A,-L} = \mathbb{E}[A^{-L}]. \tag{4.5}$$

Then, as $\rho \to \infty$, we have

$$P_{\text{out}}(\gamma_{\text{th}}) \sim P_{\text{out}}^{\text{asymp}}(\gamma_{\text{th}}, \rho), \tag{4.6}$$

where

$$P_{\text{out}}^{\text{asymp}}(\gamma_{\text{th}}, \rho) = \begin{cases} \dfrac{c_A \Gamma(L-K)}{K\Gamma(L)} \left(\dfrac{\gamma_{\text{th}}}{\rho}\right)^K, & K < L, \\ \dfrac{c_A}{\Gamma(L+1)} \left(\dfrac{\gamma_{\text{th}}}{\rho}\right)^L \log\left(\dfrac{\rho}{\gamma_{\text{th}}}\right), & K = L, \\ \dfrac{\mu_{A,-L}}{\Gamma(L+1)} \left(\dfrac{\gamma_{\text{th}}}{\rho}\right)^L, & K > L. \end{cases} \tag{4.7}$$

Consequently, the diversity order is

$$d \triangleq -\lim_{\rho\to\infty} \frac{\log P_{\text{out}}(\gamma_{\text{th}})}{\log \rho} = -\lim_{\rho\to\infty} \frac{\log P_{\text{out}}^{\text{asymp}}(\gamma_{\text{th}}, \rho)}{\log \rho} = \min(K, L). \tag{4.8}$$

Proof. Let $z = \gamma_{\text{th}}/\rho$. From the fully expanded density in (3.26) or, equivalently, from the near-origin behavior of the K-fold convolution defining f_A, the first nonzero Taylor term of $f_A(a)$ at the origin is

$$f_A(a) = c_A a^{K-1} + O(a^K), \qquad a \downarrow 0, \tag{4.9}$$

and hence

$$F_A(a) = \frac{c_A}{K} a^K + O(a^{K+1}), \qquad a \downarrow 0. \tag{4.10}$$

Let $G_L \sim \text{Gamma}(L, 1)$. For $K < L$, conditioning on G_L and using $\mathbb{E}[G_L^{-K}] = \Gamma(L-K)/\Gamma(L)$ gives

$$F_Z(z) = \mathbb{E}_{G_L}\left[F_A\left(\frac{z}{G_L}\right)\right] \sim \frac{c_A \Gamma(L-K)}{K\Gamma(L)} z^K. \tag{4.11}$$

The exchange of the limit $z \downarrow 0$ and the expectation over G_L is justified by dominated convergence. Indeed, since $F_A(x) = O(x^K)$ as $x \downarrow 0$ and $F_A(x) \le 1$ for all $x > 0$, the ratio $F_A(x)/x^K$ is bounded on $(0, \infty)$. Hence, for some constant $C > 0$, $z^{-K} F_A(z/G_L) \le C G_L^{-K}$. Since $\mathbb{E}[G_L^{-K}] < \infty$ for $K < L$, the required integrable domination follows.

For $K > L$, the negative moment $\mathbb{E}[A^{-L}]$ is finite. This follows from (4.9), because $a^{-L} f_A(a) = O(a^{K-1-L})$ is integrable at the origin when $K > L$, while A is supported on the bounded interval $[0, \sigma_{\text{tot}}]$. For completeness, substituting (3.26) into $\int_0^{\sigma_{\text{tot}}} a^{-L} f_A(a) da$ gives

$$\mu_{A,-L} = \sum_{\mathbf{q}, \mathcal{S}, \mathbf{m}_{\mathcal{S}}} \Omega(\mathbf{q}, \mathcal{S}, \mathbf{m}_{\mathcal{S}}) Q_{p(\mathbf{q}, \mathcal{S}, \mathbf{m}_{\mathcal{S}})}(\sigma_{\mathcal{S}}, \sigma_{\text{tot}}),$$

where the summation ranges are those in (3.26), and

$$Q_p(x, y) = \begin{cases} \dfrac{y^{p-L+1}}{p-L+1}, & x = 0, \\ \displaystyle\sum_{n=0}^{p} \binom{p}{n} (-x)^{p-n} \Theta_{n-L}(x, y), & x > 0, \end{cases}$$

with

$$\Theta_\eta(x,y)=\begin{cases}\dfrac{y^{\eta+1}-x^{\eta+1}}{\eta+1}, & \eta\neq -1,\\ \log\left(\dfrac{y}{x}\right), & \eta=-1.\end{cases}$$

For $\mathcal{S}=\emptyset$, the denominator $p-L+1$ is positive when $K>L$; for $\mathcal{S}\neq\emptyset$, the lower limit is positive, and the elementary antiderivatives above are finite. Since the gamma CDF satisfies $F_{G_L}(x)\sim x^L/\Gamma(L+1)$ as $x\downarrow 0$, we have

$$F_Z(z)=\mathbb{E}_A\left[F_{G_L}\left(\frac{z}{A}\right)\right]\sim\frac{z^L}{\Gamma(L+1)}\mathbb{E}[A^{-L}]. \tag{4.12}$$

Here, the exchange of the limit $z\downarrow 0$ and the expectation over A is justified by dominated convergence. The bound $F_{G_L}(x)\leq x^L/\Gamma(L+1)$ for $x\geq 0$ gives $z^{-L}F_{G_L}(z/A)\leq A^{-L}/\Gamma(L+1)$. Since $\mathbb{E}[A^{-L}]<\infty$ for $K>L$, the required integrable domination follows.

It remains to consider the boundary case $K=L$. In this case, the negative moment $\mathbb{E}[A^{-L}]$ is at the boundary of integrability. The leading logarithmic term comes from the near-origin part of the region $z<a\leq\sigma_{\mathrm{tot}}$. There, $F_{G_L}(z/a)\sim(z/a)^L/\Gamma(L+1)$ and $f_A(a)\sim c_A a^{L-1}$. Hence, the product $F_{G_L}(z/a)f_A(a)$ is asymptotically proportional to $z^L a^{-1}$. The leading logarithmic contribution can be justified by bounding the gamma CDF near the origin. Specifically, the elementary bounds $w^L/\Gamma(L+1)-w^{L+1}/((L+1)\Gamma(L))\leq F_{G_L}(w)\leq w^L/\Gamma(L+1)$ show that the correction term contributes only $O(z^L)$ after integration over $z<a\leq\sigma_{\mathrm{tot}}$. More precisely, we have

$$\int_z^{\sigma_{\mathrm{tot}}}F_{G_L}\left(\frac{z}{a}\right)f_A(a)\,da\sim\frac{c_A z^L}{\Gamma(L+1)}\int_z^{\sigma_{\mathrm{tot}}}\frac{da}{a}\sim\frac{c_A}{\Gamma(L+1)}z^L\log\left(\frac{1}{z}\right).$$

The contribution from $0<a\leq z$ is only $O(z^L)$ and is therefore asymptotically smaller than $z^L\log(1/z)$. Indeed, it is bounded above by $F_A(z)=O(z^L)$. Hence, for $K=L$, we have

$$F_Z(z)\sim\frac{c_A}{\Gamma(L+1)}z^L\log\left(\frac{1}{z}\right). \tag{4.13}$$

Substituting $z=\gamma_{\mathrm{th}}/\rho$ into (4.11)–(4.13) gives (4.7). In the balanced case, the factor $\log(\rho/\gamma_{\mathrm{th}})$ contributes only a $\log\log\rho+O(1)$ term to $\log P_{\mathrm{out}}$. Since $\log\log\rho/\log\rho\to 0$, this logarithmic factor does not change the high-SNR decay exponent. Thus, the diversity order in (4.8) follows. □

Remark 4.2. *This result shows that the diversity order of FD-STBC is limited by two structural factors: The number of transmitters K, which determines how many independent fading components are available, and the number of underlying O-STBC dimensions L, which determines how many orthogonal virtual components can be resolved by the code. Consequently, the diversity order is* $\min(K,L)$.

4.2. Bit error rate

Consider an $I\times J$ rectangular QAM constellation with Gray mapping, where $M=IJ$. We assume that I and J are powers of two and that the constellation is normalized to have the unit average symbol energy. From the general BER expression of an $I \times J$ rectangular QAM constellation [27, 34], the average BER of the considered FD-STBC system can be written as

$$P_b = \mathbb{E}_Z\left[\frac{1}{\log_2(IJ)}\left(\frac{1}{I}\sum_{u=1}^{\log_2 I} P_I(u;Z) + \frac{1}{J}\sum_{v=1}^{\log_2 J} P_J(v;Z)\right)\right] \tag{4.14}$$

where

$$\begin{aligned} P_I(u;Z) &= \sum_{i=0}^{(1-2^{-u})I-1} \Phi(i,u,I)\,\mathrm{erfc}\left(\sqrt{\frac{3(2i+1)^2\rho Z}{I^2+J^2-2}}\right), \\ P_J(v;Z) &= \sum_{j=0}^{(1-2^{-v})J-1} \Phi(j,v,J)\,\mathrm{erfc}\left(\sqrt{\frac{3(2j+1)^2\rho Z}{I^2+J^2-2}}\right), \end{aligned} \tag{4.15}$$

and

$$\Phi(i,u,I) = (-1)^{\left\lfloor \frac{i\cdot 2^{u-1}}{I}\right\rfloor}\left(2^{u-1} - \left\lfloor \frac{i\cdot 2^{u-1}}{I} + \frac{1}{2}\right\rfloor\right). \tag{4.16}$$

Here, $\gamma = \rho Z$ has already been substituted into the conditional BER expression. By the linearity of expectation, (4.14) is equivalently expressed as

$$\begin{aligned} P_b = \frac{1}{\log_2(IJ)}&\left[\frac{1}{I}\sum_{u=1}^{\log_2 I}\sum_{i=0}^{(1-2^{-u})I-1} \Phi(i,u,I)\mathbb{E}_Z\left[\mathrm{erfc}\left(\sqrt{\frac{3(2i+1)^2\rho Z}{I^2+J^2-2}}\right)\right]\right. \\ &\left.+\frac{1}{J}\sum_{v=1}^{\log_2 J}\sum_{j=0}^{(1-2^{-v})J-1} \Phi(j,v,J)\mathbb{E}_Z\left[\mathrm{erfc}\left(\sqrt{\frac{3(2j+1)^2\rho Z}{I^2+J^2-2}}\right)\right]\right]. \end{aligned} \tag{4.17}$$

Thus, the remaining channel-dependent term is the erfc expectation with respect to the exact distribution of Z. We evaluate this expectation using the gamma–beta scale-mixture law derived in Section 3. Specifically, the next lemma first evaluates the erfc average with respect to $G_L \sim \mathrm{Gamma}(L,1)$, and the subsequent theorem averages this conditional expression over the beta mixture scale A.

Lemma 4.3. *Let* $G_L \sim \mathrm{Gamma}(L,1)$*. Then, for* $x > 0$*, we have*

$$\Psi_L(x) = \mathbb{E}\left[\mathrm{erfc}\left(\sqrt{xG_L}\right)\right] = 1 - \sqrt{\frac{x}{1+x}}\sum_{\ell=0}^{L-1}\binom{2\ell}{\ell}\left(\frac{1}{4(1+x)}\right)^{\ell}. \tag{4.18}$$

Proof. We use the following integral representation of the complementary error function:

$$\mathrm{erfc}(\sqrt{y}) = \frac{2}{\pi}\int_0^{\pi/2}\exp\left(-\frac{y}{\sin^2\theta}\right)d\theta, \qquad y \geq 0. \tag{4.19}$$

This identity follows by differentiating the right-hand side with respect to y, using $u = \cot\theta$, and matching the value at $y = 0$. Therefore

$$\mathbb{E}\left[\mathrm{erfc}\left(\sqrt{xG_L}\right)\right] = \frac{2}{\pi}\int_0^{\pi/2}\left(1+\frac{x}{\sin^2\theta}\right)^{-L}d\theta. \tag{4.20}$$

Evaluating this integral gives (4.18), which is the standard maximal ratio combining (MRC) error integral for L independent diversity branches [35–37]. □

Theorem 4.4 (Exact erfc expectation for randomized signatures)**.** *For Z defined in* (2.7) *and $\tau > 0$, we have*

$$\mathbb{E}_Z\left[\operatorname{erfc}\left(\sqrt{\tau Z}\right)\right] = \mathbb{E}_A[\Psi_L(\tau A)]. \tag{4.21}$$

Proof. By Theorem 3.2, Z has the same distribution as AG_L, where A and G_L are independent. Conditioning on A and applying Lemma 4.3 yield (4.21). □

We next express the remaining expectation in (4.21) as a finite-sum closed form. For an integer $n \geq 0$, define

$$\mathcal{J}_{n,\ell}(a;\tau) = \frac{a^{n+3/2}}{n+3/2}\,{}_2F_1\left(\ell+\frac{1}{2}, n+\frac{3}{2}; n+\frac{5}{2}; -\tau a\right). \tag{4.22}$$

By the standard Gauss hypergeometric integral identity [30, Sec. 3.194] (see also [31, Ch. 15]), $\mathcal{J}_{n,\ell}(a;\tau)$ is an antiderivative of $a^{n+1/2}(1+\tau a)^{-(\ell+1/2)}$. Also define

$$\mathcal{H}_n(a;\tau) = \frac{a^{n+1}}{n+1} - \sqrt{\tau}\sum_{\ell=0}^{L-1}\frac{1}{4^\ell}\binom{2\ell}{\ell}\mathcal{J}_{n,\ell}(a;\tau), \tag{4.23}$$

and, for an integer $p \geq 0$

$$\mathcal{I}_p(b;\tau) = \sum_{n=0}^{p}\binom{p}{n}(-b)^{p-n}\left[\mathcal{H}_n(\sigma_{\text{tot}};\tau) - \mathcal{H}_n(b;\tau)\right]. \tag{4.24}$$

Theorem 4.5 (Fully expanded closed-form erfc expectation)**.** *For $L \geq 2$ and $\tau > 0$*

$$\mathbb{E}_Z\left[\operatorname{erfc}\left(\sqrt{\tau Z}\right)\right] = \sum_{\mathbf{q}\in\{0,\ldots,L-2\}^K}\sum_{\mathcal{S}\subseteq\mathcal{K}}\sum_{\mathbf{m}_\mathcal{S}\in\mathcal{M}(\mathcal{S},\mathbf{q})}\Omega(\mathbf{q},\mathcal{S},\mathbf{m}_\mathcal{S})\mathcal{I}_{p(\mathbf{q},\mathcal{S},\mathbf{m}_\mathcal{S})}(\sigma_\mathcal{S};\tau). \tag{4.25}$$

Therefore, the erfc expectation in the rectangular QAM BER expression is a finite sum of elementary powers and Gauss hypergeometric functions, with no residual stochastic expectation or numerical quadrature.

Proof. Substituting $x = \tau a$ into (4.18) gives

$$\Psi_L(\tau a) = 1 - \sqrt{\tau a}\sum_{\ell=0}^{L-1}\frac{1}{4^\ell}\binom{2\ell}{\ell}(1+\tau a)^{-(\ell+1/2)}. \tag{4.26}$$

Hence $\mathcal{H}_n(a;\tau)$ is an antiderivative of $a^n\Psi_L(\tau a)$. Substituting the expanded density (3.26) into (4.21) yields integrals over $0 \leq a \leq \sigma_{\text{tot}}$. Since, for each term, $(a-\sigma_\mathcal{S})_+^{p(\mathbf{q},\mathcal{S},\mathbf{m}_\mathcal{S})} = 0$ when $a < \sigma_\mathcal{S}$, these integrals can be written as

$$\mathbb{E}_Z\left[\operatorname{erfc}\left(\sqrt{\tau Z}\right)\right] = \sum_{\mathbf{q}}\sum_{\mathcal{S}}\sum_{\mathbf{m}_\mathcal{S}}\Omega(\mathbf{q},\mathcal{S},\mathbf{m}_\mathcal{S})\int_{\sigma_\mathcal{S}}^{\sigma_{\text{tot}}}(a-\sigma_\mathcal{S})^{p(\mathbf{q},\mathcal{S},\mathbf{m}_\mathcal{S})}\Psi_L(\tau a)da. \tag{4.27}$$

For a fixed term, put $b = \sigma_\mathcal{S}$ and $p = p(\mathbf{q},\mathcal{S},\mathbf{m}_\mathcal{S})$. Then

$$(a-b)^p = \sum_{n=0}^{p}\binom{p}{n}(-b)^{p-n}a^n \tag{4.28}$$

over the interval $b \leq a \leq \sigma_{\text{tot}}$. Since $\mathcal{H}_n(a;\tau)$ is an antiderivative of $a^n\Psi_L(\tau a)$, the integral in (4.27) becomes $\mathcal{I}_p(b;\tau)$. This gives (4.25). □

Thus, for each QAM distance parameter

$$\tau_i^{(I)} = \frac{3(2i+1)^2\rho}{I^2+J^2-2}, \qquad \tau_j^{(J)} = \frac{3(2j+1)^2\rho}{I^2+J^2-2}, \tag{4.29}$$

the corresponding expectation $\mathbb{E}_Z[\operatorname{erfc}(\sqrt{\tau Z})]$ in (4.17) is evaluated by (4.25). Consequently, substituting these closed-form expectations into (4.17) gives the analytical BER expression.

4.2.1. Approximate BER expression

For high-SNR interpretation, we also consider a simplified BER expression based on the nearest-neighbor approximation for rectangular QAM. This approximation retains only the dominant minimum distance error terms and neglects error events associated with further constellation points. Applying this approximation [34, Eq (23)] to (4.17) gives

$$P_b^{\text{approx}}(\rho) = \frac{1}{\log_2(IJ)}\left(\frac{I-1}{I} + \frac{J-1}{J}\right)\mathbb{E}_Z\left[\operatorname{erfc}\left(\sqrt{\frac{3\rho Z}{I^2+J^2-2}}\right)\right]. \tag{4.30}$$

Therefore, the approximate BER requires only one evaluation of the closed-form erfc expectation in (4.25). For $M = 2$ and $M = 4$, the exact BER expression in (4.17) contains only the minimum distance error terms retained in (4.30), so the exact and approximate BER expressions coincide for all SNRs. For higher-order modulations, the exact expression additionally contains error terms associated with further constellation points. Neglecting these terms causes the approximation to deviate from the exact BER, particularly at a low SNR and for larger modulation orders, consistent with the general QAM BER analysis in [34].

5. Numerical experiments

We verify the derived closed-form expressions by comparing the corresponding analytical curves with Monte Carlo simulation results across various parameter settings. The purpose of the numerical experiments is not to introduce an additional approximation, but to verify that the mathematical expressions for the PDF, CDF, outage probability, and BER reproduce the corresponding Monte Carlo results. The agreement between the analytical curves and simulation results, therefore, supports the gamma–beta scale-mixture law as an exact description under the considered FD-STBC model.

All numerical experiments were performed in MATLAB. Independent complex unit-hyperspherical signature vectors and fading coefficients were generated for each Monte Carlo realization. In the BER simulations, these random quantities were regenerated independently for each transmitted O-STBC block and held fixed over the block. The O-STBC codewords were those given in Examples 2.2 and 2.3 of Section 2.2. The PDF and outage probability experiments used 10^9 independent Monte Carlo realizations for each parameter configuration, whereas the BER experiments used 10^9 information bits at each SNR point for each parameter configuration. The PDF histograms were constructed using equal-width bins and normalized to unit area. The figure-specific values of K, L, M, ρ_{tot}, and γ_{th} are given in the corresponding figure captions and discussions.

5.1. Validation of the analytical expressions

The fully expanded formulas in (3.35), (3.36), (4.3), (4.7), and (4.17) with (4.25) contain only finite sums and standard special functions. Therefore, for fixed $K, L, M, \rho, \gamma_{\text{th}}$, and $\{\sigma_k\}$, the analytical outage probability and BER can be obtained by direct finite-sum evaluation without simulating $\mathbf{R}$, $\mathbf{h}$, or the mixing variable A. The numerical experiments focus on practical cooperative group sizes. Since the number of simultaneous cooperating nodes in distributed cooperative transmission is typically limited by power consumption, scheduling overhead, and resource-sharing constraints, the selected values of K correspond to operationally relevant FD-STBC scenarios. When the numerical plots use the total network SNR $\rho_{\text{tot}} = P_{\text{tot}}/N_0$ as the horizontal axis, the analytical SNR is evaluated by the substitution $\rho = (T/N)\rho_{\text{tot}}/K$, consistent with the power normalization in Proposition 2.1. Unless otherwise stated, we consider equal average channel powers, $\sigma_k = 1$ for all k. This symmetric setting isolates the effects of the number of transmitters K, the number of virtual transmit dimensions L, and the modulation order M, while the derived formulas themselves remain valid for arbitrary positive $\{\sigma_k\}$.

First, Figure 1 validates the distributional characterization of the effective channel gain, which is one of the central objectives of this paper, by comparing the exact PDF in (3.35) with the Monte Carlo histograms of $Z = \|\mathbf{Rh}\|^2$. The comparison is performed for $K \in \{2, 3, 4, 5\}$ and $L \in \{2, 3, 4\}$. In this experiment, the random signature vectors are generated by normalizing independent complex Gaussian vectors, and the fading vector is generated as $\mathbf{h} \sim \mathcal{CN}(\mathbf{0}, \Sigma)$ with $\Sigma = \mathbf{I}_K$. The close agreement between the analytical curves and the histograms confirms that the derived PDF accurately captures the distribution of the effective channel gain in the FD-STBC system.

Figures 2 and 3 validate the outage probability expression from two complementary viewpoints. Since the outage probability is obtained directly from the CDF $F_Z(z)$, the analytical curves in both figures are computed from the exact CDF-based outage expression in (4.3), whereas the simulation markers are generated by Monte Carlo simulations. The two experiments differ only in the swept variable: Figure 2 varies the total network SNR $\rho_{\text{tot}} = P_{\text{tot}}/N_0$, whereas Figure 3 varies the outage threshold γ_{th}. Following Proposition 2.1, the analytical SNR is $\rho = (T/N)\rho_{\text{tot}}/K$, so the post-combining received SNR is $\gamma = \rho Z = \rho_{\text{tot}}(T/N)Z/K$. Thus, the outage event $\gamma < \gamma_{\text{th}}$ is evaluated through the CDF argument

$$z_{\text{th}} = \frac{\gamma_{\text{th}}}{\rho} = \frac{K\gamma_{\text{th}}}{(T/N)\rho_{\text{tot}}}. \tag{5.1}$$

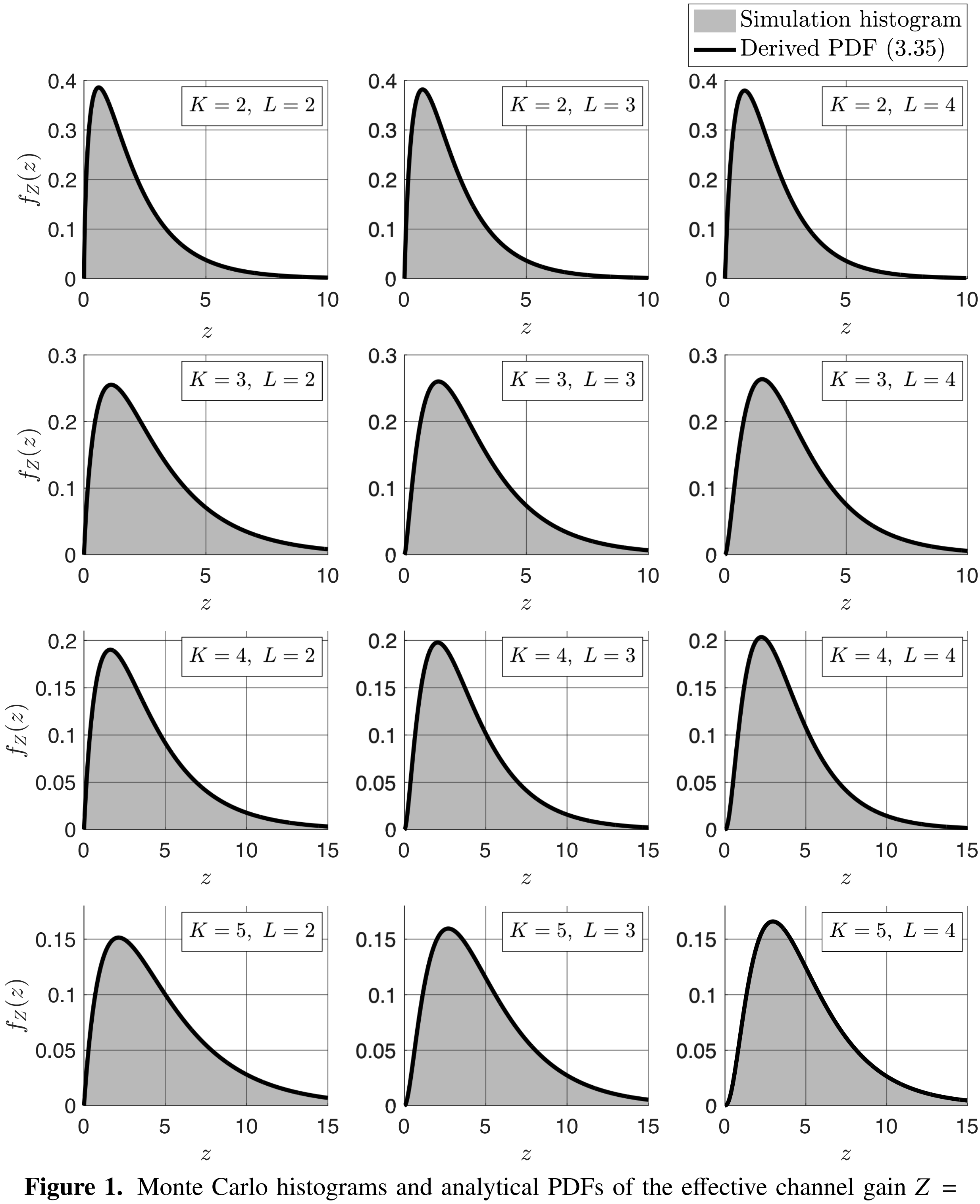

Figure 1. Monte Carlo histograms and analytical PDFs of the effective channel gain $Z = ||\mathbf{Rh}||^2$ for $K \in \{2, 3, 4, 5\}$, $L \in \{2, 3, 4\}$, and $\sigma_k = 1$ for all k.

Figure 2 shows the outage probability as a function of ρ_{tot} for the fixed threshold $\gamma_{\text{th}} = 1$, corresponding to a 0-dB post-combining SNR threshold. This figure verifies both the exact outage probability expression and the high-SNR diversity behavior. The solid curves represent the exact analytical outage probabilities in (4.3), while the dotted curves represent the asymptotic references obtained from (4.7). The close agreement between the simulation markers and the exact analytical curves confirms that the derived CDF-based outage probability expression accurately describes the outage probability of the FD-STBC system. For comparison with the closest prior analytical result, Figure 2(a) also includes the outage upper bound (UB) derived in [10, (16)] for the special case $K = L = 2$. The upper bound lies above both the exact analytical curve and the Monte Carlo estimates, highlighting the extension from the previous upper-bound characterization for $K = L = 2$ to the present exact outage expression for an arbitrary K and L. Furthermore, the asymptotic curves show that the high-SNR decay slopes are consistent with the predicted diversity order $d = \min(K, L)$ in (4.8). In the balanced case $K = L$, the leading term contains a logarithmic correction of the form $\rho^{-L} \log \rho$ or, equivalently, $\rho_{\text{tot}}^{-L} \log \rho_{\text{tot}}$ up to constant factors under $\rho = (T/N)\rho_{\text{tot}}/K$, which slows convergence to the asymptotic slope. For this reason, the balanced-case asymptotic references are shown only in the high-SNR region.

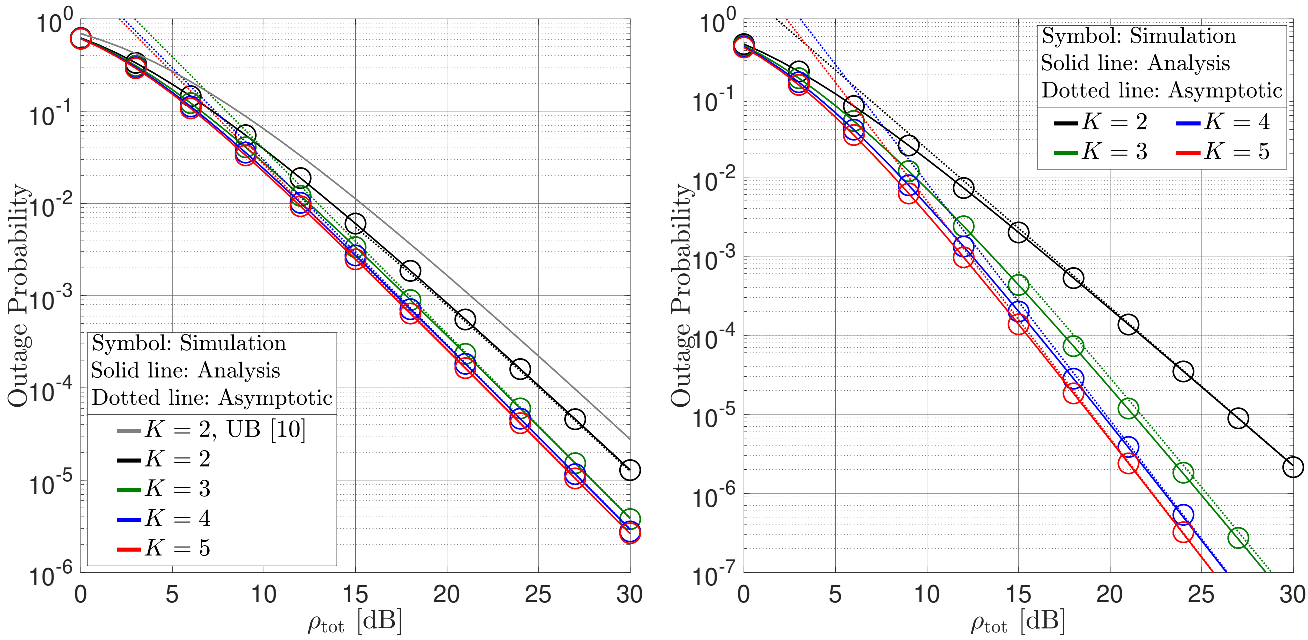

(a) $L = 2$

(b) $L = 3$

Figure 2. Outage probability versus total network SNR $\rho_{\text{tot}} = P_{\text{tot}}/N_0$ for the received SNR threshold $\gamma_{\text{th}} = 1$, $K \in \{2, 3, 4, 5\}$, $L \in \{2, 3\}$, and $\sigma_k = 1$ for all k. Symbols denote Monte Carlo simulations and solid lines denote the exact CDF-based outage expression in (4.3). The asymptotic references are obtained from (4.7) and illustrate the diversity order $d = \min(K, L)$.

Figure 3 fixes $\rho_{\text{tot}} = 10$ dB and varies the received SNR threshold γ_{th}. This threshold sweep experiment directly traces the dependence of the outage probability on the CDF. Specifically, for a fixed ρ_{tot}, increasing γ_{th} moves the evaluation point z_{th} in (5.1), so the resulting outage curve follows the shape of the CDF $F_Z(z)$ under the corresponding scaling. The range $\gamma_{\text{th}} \in [-10, 20]$ dB or, equivalently, $0.1 \leq \gamma_{\text{th}} \leq 100$, covers a broad set of received SNR thresholds from lenient to stringent reliability requirements. The agreement between simulation markers and analytical curves over this range verifies that the derived CDF accurately captures the outage behavior not only along the SNR axis, but also across different reliability thresholds.

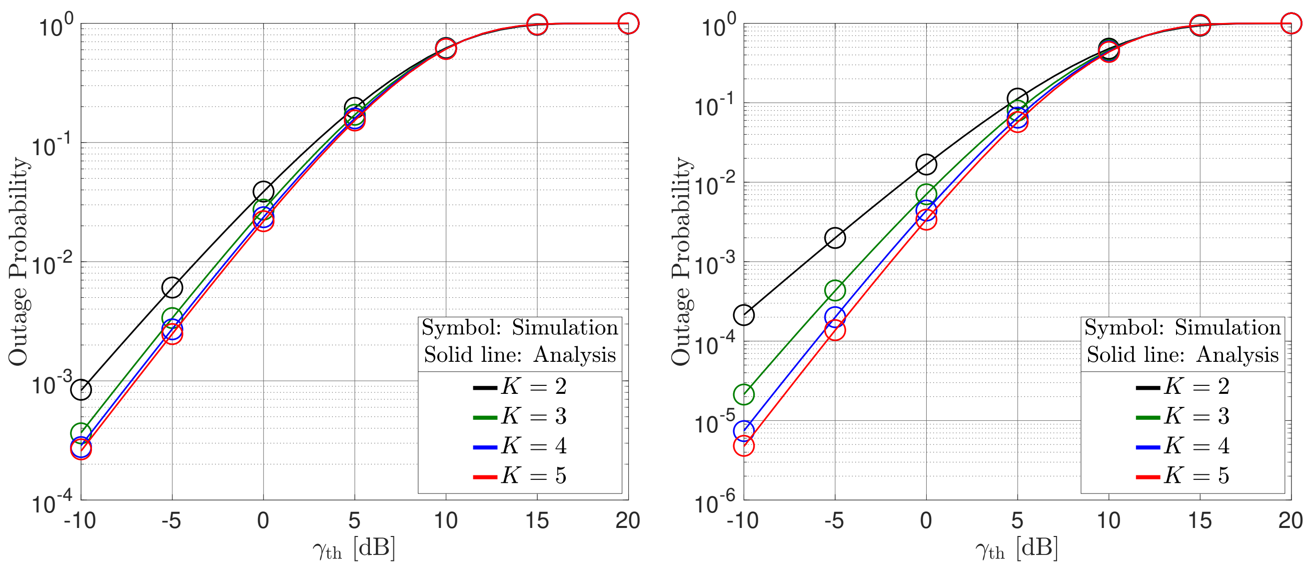

(a) $L = 2$

(b) $L = 3$

Figure 3. Outage probability versus the received SNR threshold γ_{th}, shown on a dB scale, at a fixed total network SNR $\rho_{\mathrm{tot}} = 10$ dB for $K \in \{2, 3, 4, 5\}$, $L \in \{2, 3\}$, and $\sigma_k = 1$ for all k. Symbols denote Monte Carlo simulations and solid lines denote the exact CDF-based outage expression evaluated at the scaled threshold $K\gamma_{\mathrm{th}}/((T/N)\rho_{\mathrm{tot}})$.

Finally, Figures 4 and 5 validate the derived BER expression for the complete FD-STBC transmission model. Unlike the outage experiments, which are based solely on the random variable Z, the BER simulation generates information symbols, hyperspherical signature vectors, wireless channel coefficients, and AWGN samples and then applies the corresponding O-STBC combiner. Thus, the Monte Carlo BER is obtained from an end-to-end FD-STBC transceiver simulation, independently of the closed-form BER formula, and is computationally more demanding. For the SNR axis $\rho_{\mathrm{tot}} = P_{\mathrm{tot}}/N_0$, all transmitters use the same time-averaged transmit power P_{tot}/K. Equivalently, the rate-N/T O-STBC power compensation gives the codeword-level scaling coefficient $P_{\mathrm{c}} = (T/N)(P_{\mathrm{tot}}/K)$. Hence, the analytical BER is evaluated with the same SNR substitution $\rho = P_{\mathrm{c}}/N_0 = (T/N)\rho_{\mathrm{tot}}/K$ used in the outage evaluation. The same normalization is used in the transceiver simulation.

Figures 4 and 5 correspond to $L = 2$ and $L = 3$, respectively. In each figure, the four subfigures show modulation orders $M \in \{2, 4, 8, 16\}$, and each subfigure compares $K \in \{2, 3, 4, 5\}$. The case $M = 2$ can be interpreted as binary phase-shift keying (BPSK), as in [9], while the other cases correspond to rectangular QAM constellations. The solid curves are obtained from the exact BER expression in (4.17), while the dotted curves are obtained from the approximate BER expression in (4.30). The simulation markers closely match the analytical BER curves across all tested values of K, L, and M, confirming that the derived distribution of Z accurately predicts the BER of the FD-STBC system. For $M = 2$ and $M = 4$, the approximate and exact BER expressions coincide. For $M = 8$ and $M = 16$, the approximation slightly underestimates the exact BER, and this discrepancy becomes more pronounced in the low-SNR region. At medium to high SNR, the approximate curves nearly overlap the exact curves, showing that the nearest-neighbor approximation captures the dominant error behavior in this regime.

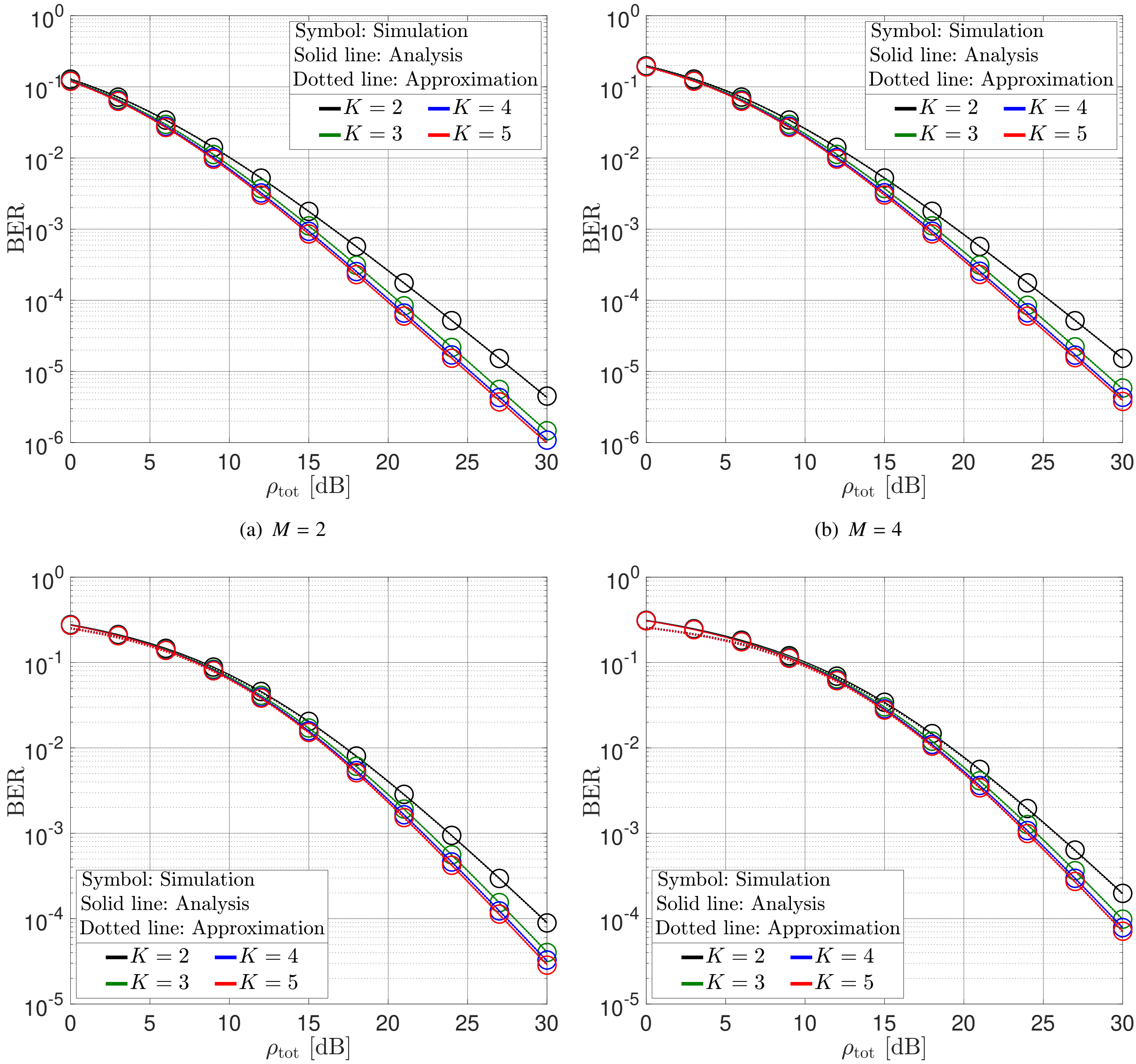

(a) $M = 2$ (b) $M = 4$

(c) $M = 8$ (d) $M = 16$

Figure 4. BER versus total network SNR $\rho_{\text{tot}} = P_{\text{tot}}/N_0$ for $L = 2$, $K \in \{2, 3, 4, 5\}$, $\sigma_k = 1$, and modulation orders $M \in \{2, 4, 8, 16\}$. Symbols denote Monte Carlo simulations, solid lines denote the exact analytical BER, and dotted lines denote the approximate BER.

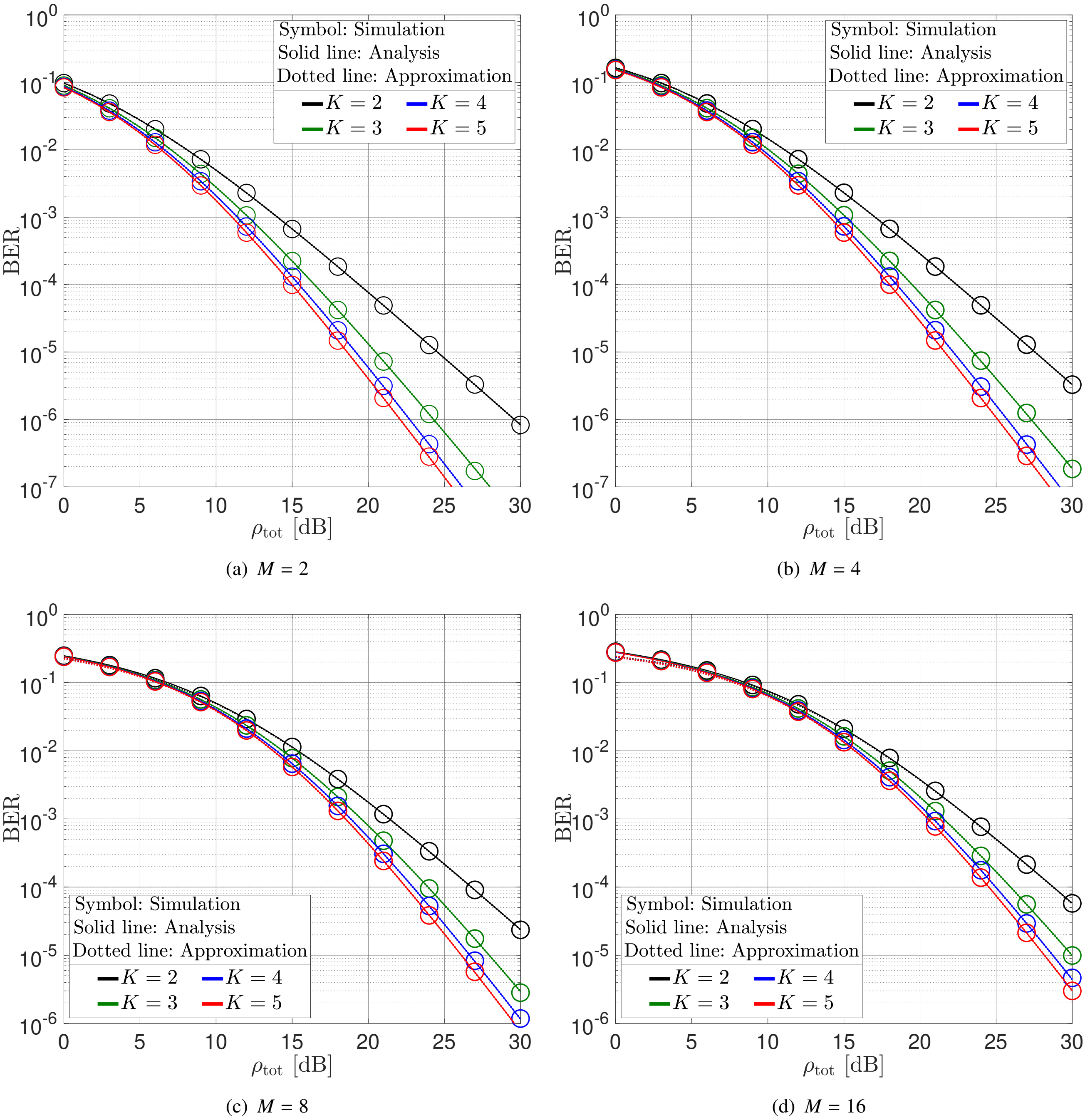

(a) $M = 2$ (b) $M = 4$

(c) $M = 8$ (d) $M = 16$

Figure 5. BER versus total network SNR $\rho_{\mathrm{tot}} = P_{\mathrm{tot}}/N_0$ for $L = 3$, $K \in \{2, 3, 4, 5\}$, $\sigma_k = 1$, and modulation orders $M \in \{2, 4, 8, 16\}$. Symbols denote Monte Carlo simulations, solid lines denote the exact analytical BER, and dotted lines denote the approximate BER.

5.2. Computational considerations

Beyond validating the analytical expressions, the numerical experiments also provide a basis for comparing the term counts of the finite-sum formulas with the sample requirements of Monte Carlo evaluations. For each parameter configuration, the PDF and outage probability experiments use 10^9

independent realizations and the BER experiments use 10^9 information bits at each SNR point. Thus, an outage probability or BER on the order of 10^{-7} corresponds to an expected count on the order of only 10^2 outage events or bit errors, illustrating the large sample requirement of rare-event Monte Carlo evaluations. The computational effort per Monte Carlo realization also increases with K and L, since each realization requires generating and processing K length-L signatures and the associated channel coefficients and, for BER evaluation, simulating the corresponding O-STBC block.

Proposition 3.9 bounds the number of base and n-indexed terms in the expanded PDF by $K(L-1)N_{\text{base}}(K, L)$. For each base term, the finite sum defining $\mathcal{I}_{p(\mathbf{q},\mathcal{S},\mathbf{m}_{\mathcal{S}})}$ in (4.24) contains at most $K(L-1)$ terms, so the same term-count bound applies to each closed-form erfc expectation in (4.25). The expanded CDF, and hence the outage probability expression, contains at most $LK(L-1)N_{\text{base}}(K, L)$ such terms. For $M = 2$ and $M = 4$, a single such erfc expectation suffices for the exact BER, whereas higher-order modulations require additional expectations associated with far constellation points. Table 4 reports this upper bound for selected (K, L) pairs, showing that it remains comparatively modest for smaller K and L but increases sharply as both K and L grow. These values are finite-sum term-count bounds rather than arithmetic operation counts, since individual terms may involve special-function evaluations. Direct deterministic evaluation can therefore be useful at small and moderate (K, L), particularly for rare-event probabilities, high numerical accuracy, or repeated parameter evaluations, because it avoids Monte Carlo sampling error, and its term count is independent of the target probability. At larger K and L, however, the rapidly increasing finite-sum size can offset this advantage, and Monte Carlo simulation or the convolution and quadrature alternative described in Section 3.4 may become preferable.

Table 4. Representative values of the upper bound $K(L-1)N_{\text{base}}(K, L)$ on the number of base and n-indexed terms for selected values of K and L.

	$K = 2$	$K = 3$	$K = 5$	$K = 10$
$L = 2$	8	24	160	10,240
$L = 3$	100	750	31,250	195,312,500
$L = 4$	486	6,561	885,735	104,603,532,030

6. Conclusions

In this paper, we characterized the exact probability distribution of the squared norm of a sum of complex-Gaussian-scaled hyperspherical random vectors, which arises as the effective channel gain of FD-STBC with independent complex unit-hyperspherical signatures. By analyzing the effective channel vector directly, we obtained the gamma–beta scale-mixture law $Z \stackrel{d}{=} AG_L$, where the gamma component is the squared norm of an isotropic complex Gaussian vector, and the compactly supported mixing variable A is a weighted sum of independent beta random variables. This representation yields deterministic formulas for both the associated distributional quantities and the performance metrics of the FD-STBC application. Specifically, we derived a fully expanded density for the mixing variable, finite-sum closed-form expressions for the PDF and CDF of the effective channel gain, its exact Laplace transform, closed-form moments, and analytical expressions for outage probability and BER. For small and moderate values of K and L, these formulas allow the corresponding quantities to be evaluated directly using finite sums and standard special functions, without repeated Monte Carlo averaging over random signatures and fading coefficients. We further quantified the growth of the finite expansions, clarified the regimes in which direct evaluation remains practical, and identified a convolution and quadrature alternative. The high-SNR outage expansion further showed that the diversity order is $\min(K, L)$. Numerical experiments validated the derived law and the resulting analytical expressions by comparing the analytical PDF, CDF-based outage probability, high-SNR diversity behavior, and BER with independent Monte Carlo simulations. Thus, the derived gamma–beta scale-mixture law provides an exact distributional construction with direct computational value, while FD-STBC serves as a concrete engineering application of the framework. These results provide a distribution theoretic basis, validated by Monte Carlo simulations, for evaluating FD-STBC systems with complex unit-hyperspherical signatures. The resulting framework may also serve as an analytical basis for subsequent studies of FD-STBC, including generalized BRNs and distributed cooperative satellite communication scenarios.

Author contributions

Ki-Hun Lee: Conceptualization, methodology, software, formal analysis, investigation, data curation, writing – original draft, visualization, project administration; Nam-Jin Park: Methodology, validation, investigation, resources, supervision, writing – review and editing. All authors have read and approved the final version of the manuscript for publication.

Use of Generative-AI tools declaration

The authors declare they have not used artificial intelligence (AI) tools in the creation of this article.

Acknowledgments

This work was supported in part by a Korea University Grant and in part by the Basic Science Research Program through the National Research Foundation of Korea (NRF) funded by the Ministry of Education (No. RS-2025-25415939).

Conflict of interest

All authors declare no conflicts of interest in this paper.

References

1. M. Kang, M.-S. Alouini, Largest eigenvalue of complex Wishart matrices and performance analysis of MIMO MRC systems, *IEEE J. Sel. Areas Commun.*, **21** (2003), 418–426. https://doi.org/10.1109/JSAC.2003.809720
2. S. Kotz, N. Balakrishnan, N. L. Johnson, *Continuous multivariate distributions: Models and applications*, John Wiley & Sons, Inc., 2000. https://doi.org/10.1002/0471722065
3. R. J. Muirhead, *Aspects of multivariate statistical theory*, John Wiley & Sons, Inc., 1982. https://doi.org/10.1002/9780470316559

4. V. Tarokh, H. Jafarkhani, A. R. Calderbank, Space-time block codes from orthogonal designs, *IEEE Trans. Inf. Theory*, **45** (1999), 1456–1467. https://doi.org/10.1109/18.771146

5. S. M. Alamouti, A simple transmit diversity technique for wireless communications, *IEEE J. Sel. Areas Commun.*, **16** (1998), 1451–1458. https://doi.org/10.1109/49.730453

6. J. N. Laneman, G. W. Wornell, Distributed space-time-coded protocols for exploiting cooperative diversity in wireless networks, *IEEE Trans. Inf. Theory*, **49** (2003), 2415–2425. https://doi.org/10.1109/TIT.2003.817829

7. J. N. Laneman, D. N. C. Tse, G. W. Wornell, Cooperative diversity in wireless networks: Efficient protocols and outage behavior, *IEEE Trans. Inf. Theory*, **50** (2004), 3062–3080. https://doi.org/10.1109/TIT.2004.838089

8. S. Yiu, R. Schober, L. Lampe, Distributed space-time block coding, *IEEE Trans. Commun.*, **54** (2006), 1195–1206. https://doi.org/10.1109/TCOMM.2006.877947

9. B. Sirkeci-Mergen, A. Scaglione, Randomized space-time coding for distributed cooperative communication, *IEEE Trans. Signal Process.*, **55** (2007), 5003–5017. https://doi.org/10.1109/TSP.2007.896061

10. K.-H. Lee, H. Lee, J. Choi, S. Park, B. C. Jung, Distributed space-time block coding for barrage relay networks, In: *MILCOM 2023 - 2023 IEEE military communications conference (MILCOM)*, Boston: IEEE, 2023, 292–297. https://doi.org/10.1109/MILCOM58377.2023.10356386

11. K. V. Mardia, P. E. Jupp, *Directional statistics*, John Wiley & Sons, Inc., 2000. https://doi.org/10.1002/9780470316979

12. M. D. Springer, W. E. Thompson, The distribution of products of beta, gamma and Gaussian random variables, *SIAM J. Appl. Math.*, **18** (1970), 721–737. https://doi.org/10.1137/0118065

13. R. E. Gaunt, Products of normal, beta and gamma random variables: Stein operators and distributional theory, *Braz. J. Probab. Stat.*, **32** (2018), 437–466. https://doi.org/10.1214/16-BJPS349

14. J. Pitman, M. Z. Rácz, Beta-gamma tail asymptotics, *Electron. Commun. Probab.*, **20** (2015), 1–7. https://doi.org/10.1214/ECP.v20-4545

15. S. B. Provost, Y.-H. Cheong, On the distribution of linear combinations of the components of a Dirichlet random vector, *Can. J. Stat.*, **28** (2000), 417–425. https://doi.org/10.2307/3315988

16. T. Pham-Gia, N. Turkkan, Distribution of the linear combination of two general beta variables and applications, *Commun. Stat. Theory Methods*, **27** (1998), 1851–1869. https://doi.org/10.1080/03610929808832194

17. S. Nadarajah, X. Jiang, J. Chu, A saddlepoint approximation to the distribution of the sum of independent non-identically beta random variables, *Stat. Neerl.*, **69** (2015), 102–114. https://doi.org/10.1111/stan.12051

18. H. Homei, S. Nadarajah, On products and mixed sums of gamma and beta random variables motivated by availability, *Methodol. Comput. Appl. Probab.*, **20** (2018), 799–810. https://doi.org/10.1007/s11009-017-9591-2

19. F. Verde, D. Darsena, A. Scaglione, Cooperative randomized MIMO-OFDM downlink for multicell networks: Design and analysis, *IEEE Trans. Signal Process.*, **58** (2010), 384–402. https://doi.org/10.1109/TSP.2009.2030837

20. T. Q. Duong, Ö. Alay, E. Erkip, H.-J. Zepernick, End-to-end performance of randomized distributed space-time codes, In: *21st Annual IEEE international symposium on personal, indoor and mobile radio communications*, IEEE, Istanbul, 2010, 988–993. https://doi.org/10.1109/PIMRC.2010.5671575

21. J. Soffritti, H.-J. Zepernick, M. L. Merani, Performance analysis of randomized distributed space-time codes in Nakagami-m fading, In: *2013 International conference on advanced technologies for communications (ATC 2013)*, Vietnam: IEEE, 2013, 408–413. https://doi.org/10.1109/ATC.2013.6698146

22. J. Soffritti, T. Q. Duong, M. L. Merani, H.-J. Zepernick, Performance analysis of randomized distributed space-time codes over composite Gamma/lognormal fading channels, In: *2014 IEEE 80th vehicular technology conference (VTC2014-Fall)*, Canada: IEEE, 2014, 1–5. https://doi.org/10.1109/VTCFall.2014.6966117

23. Ö. Alay, P. Liu, Y. Wang, E. Erkip, S. S. Panwar, Cooperative layered video multicast using randomized distributed space time codes, *IEEE Trans. Multimedia*, **13** (2011), 1127–1140. https://doi.org/10.1109/TMM.2011.2158088

24. F. Verde, Performance analysis of randomised space-time block codes for amplify-and-forward cooperative relaying, *IET Commun.*, **7** (2013), 1883–1898. https://doi.org/10.1049/iet-com.2013.0170

25. D. Gregoratti, W. Hachem, X. Mestre, Randomized isometric linear-dispersion space-time block coding for the DF relay channel, *IEEE Trans. Signal Process.*, **60** (2012), 426–442. https://doi.org/10.1109/TSP.2011.2171685

26. K. Lu, S. Fu, X.-G. Xia, Closed-form designs of complex orthogonal space-time block codes of rates $(k+1)/(2k)$ for $2k-1$ or $2k$ transmit antennas, *IEEE Trans. Inf. Theory*, **51** (2005), 4340–4347. https://doi.org/10.1109/TIT.2005.858943

27. K.-H. Lee, K. Lim, B. C. Jung, STEALTH: Space-time encryption via constellation hiding for MIMO two-way untrusted relay systems, *IEEE Internet Things J.*, **12** (2025), 30319–30334. https://doi.org/10.1109/JIOT.2025.3571736

28. A. M. Mathai, S. B. Provost, *Quadratic forms in random variables: Theory and applications*, New York: Marcel Dekker, 1992.

29. A. W. van der Vaart, *Asymptotic statistics*, Cambridge University Press, 1998. https://doi.org/10.1017/CBO9780511802256

30. I. S. Gradshteyn, I. M. Ryzhik, *Table of integrals, series, and products*, Academic Press, 2014. https://doi.org/10.1016/C2010-0-64839-5

31. F. W. J. Olver, D. W. Lozier, R. F. Boisvert, C. W. Clark, *NIST handbook of mathematical functions*, New York: Cambridge University Press, 2010.

32. H. M. Srivastava, P. W. Karlsson, *Multiple Gaussian hypergeometric series*, 1985.

33. Q. Shi, Y. Karasawa, Some applications of Lauricella hypergeometric function F_A in performance analysis of wireless communications, *IEEE Commun. Lett.*, **16** (2012), 581–584. https://doi.org/10.1109/LCOMM.2012.030912.112454

34. K. Cho, D. Yoon, On the general BER expression of one- and two-dimensional amplitude modulations, *IEEE Trans. Commun.*, **50** (2002), 1074–1080. https://doi.org/10.1109/TCOMM.2002.800818

35. D. Tse, P. Viswanath, *Fundamentals of wireless communication*, Cambridge University Press, 2005. https://doi.org/10.1017/CBO9780511807213

36. J. W. Craig, A new, simple and exact result for calculating the probability of error for two-dimensional signal constellations, In: *MILCOM 91 - Conference record*, McLean: IEEE, **2** (1991), 571–575. https://doi.org/10.1109/MILCOM.1991.258319

37. M. K. Simon, M.-S. Alouini, *Digital communication over fading channels*, John Wiley & Sons, Inc., 2004. https://doi.org/10.1002/0471715220

AIMS Press